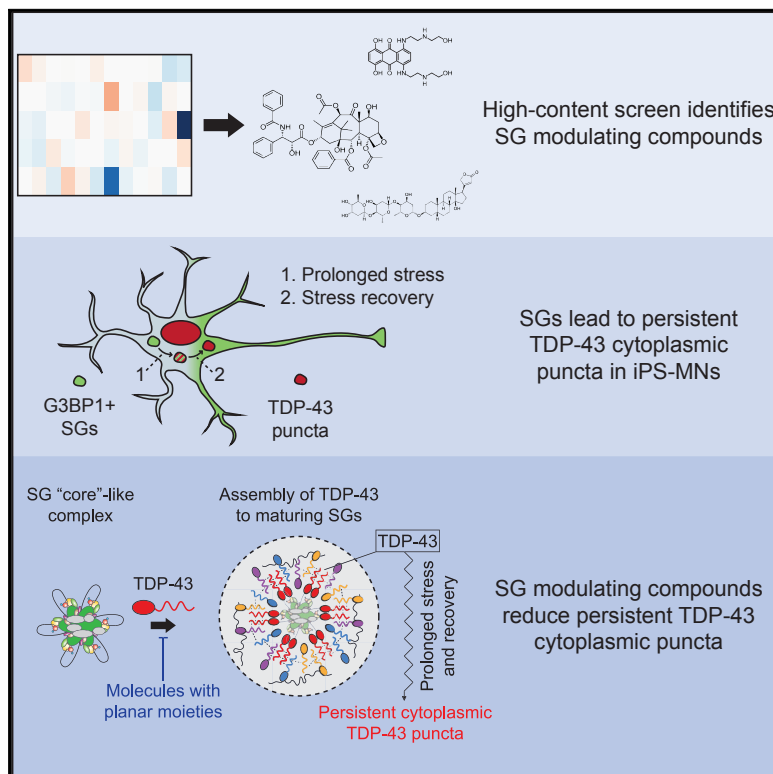


Small-Molecule Modulation of TDP-43 Recruitment to Stress Granules Prevents Persistent TDP-43 Accumulation in ALS/FTD

Graphical Abstract



Authors

Mark Y. Fang, Sebastian Markmiller,
Anthony Q. Vu, ..., Eric Lecuyer,
Joseph W. Lewcock, Gene W. Yeo

Correspondence

geneyeo@ucsd.edu

In Brief

Using high-content screening, we identified a class of planar small molecules that can (1) modulate the dynamics of neurodegeneration-linked stress granules (SGs), (2) reduce SG association of ALS-linked RNA-binding proteins, and (3) prevent accumulation of TDP-43 within persistent cytoplasmic puncta.

Highlights

- ~100 small-molecule compounds modulate SGs in HEK293xT cells, NPCs, and iPS-MNs
- ALS-associated RBPs accumulate in SGs during prolonged stress
- Molecules with planar moieties disrupt accumulation of ALS-associated RBPs in SGs
- Compounds reduce TDP-43 accumulation in cytoplasmic puncta in ALS mutant iPS-MNs

Small-Molecule Modulation of TDP-43 Recruitment to Stress Granules Prevents Persistent TDP-43 Accumulation in ALS/FTD

Mark Y. Fang,^{1,2,3} Sebastian Markmiller,^{1,2,3} Anthony Q. Vu,^{1,2,3} Ashkan Javaherian,⁴ William E. Dowdle,^{5,14} Philippe Jolivet,⁶ Paul J. Bushway,^{7,13,15} Nicholas A. Castello,⁴ Ashmita Baral,⁴ Michelle Y. Chan,⁴ Jeremy W. Linsley,⁴ Drew Linsley,⁸ Mark Mercola,^{7,13,16} Steven Finkbeiner,^{9,10} Eric Lecuyer,^{6,11,12} Joseph W. Lewcock,⁵ and Gene W. Yeo^{1,2,3,17,*}

¹Department of Cellular and Molecular Medicine, University of California, San Diego, La Jolla, CA 92093, USA

²Stem Cell Program, University of California, San Diego, La Jolla, CA 92093, USA

³Institute for Genomic Medicine, University of California, San Diego, La Jolla, CA 92093, USA

⁴Gladstone Institutes, San Francisco, CA 94158, USA

⁵Denali Therapeutics Inc., South San Francisco, CA 94080, USA

⁶Institut de Recherches Cliniques de Montréal, Montréal, Québec H2W 1R7, Canada

⁷Sanford Burnham Prebys Medical Discovery Institute, La Jolla, CA 92037, USA

⁸Brown University, Department of Cognitive, Linguistic and Psychological Sciences, Providence, RI 02912, USA

⁹Taube/Koret Center for Neurodegenerative Disease Research and DaedalusBio, Gladstone Institutes, San Francisco, CA 94158, USA

¹⁰Departments of Neurology and Physiology, University of California, San Francisco, San Francisco, CA 94158, USA

¹¹Département de Biochimie et Médecine Moléculaire, Université de Montréal, Montréal, Québec H3C 3J7, Canada

¹²Division of Experimental Medicine, McGill University, Montréal, Québec H3A 1A3, Canada

¹³Department of Bioengineering, University of California, San Diego, La Jolla, CA 92093

¹⁴Present address: Maze Therapeutics, San Francisco, CA 94158, USA

¹⁵Present address: Department of Bioengineering, Jacobs School of Engineering, University of California, San Diego, La Jolla, CA 92093, USA

¹⁶Present address: Stanford Cardiovascular Institute and Department of Medicine, Stanford University, Stanford, CA 94305, USA

¹⁷Lead Contact

*Correspondence: geneyeo@ucsd.edu

<https://doi.org/10.1016/j.neuron.2019.05.048>

SUMMARY

Stress granules (SGs) form during cellular stress and are implicated in neurodegenerative diseases such as amyotrophic lateral sclerosis and frontotemporal dementia (ALS/FTD). To yield insights into the role of SGs in pathophysiology, we performed a high-content screen to identify small molecules that alter SG properties in proliferative cells and human iPSC-derived motor neurons (iPS-MNs). One major class of active molecules contained extended planar aromatic moieties, suggesting a potential to intercalate in nucleic acids. Accordingly, we show that several hit compounds can prevent the RNA-dependent recruitment of the ALS-associated RNA-binding proteins (RBPs) TDP-43, FUS, and HNRNPA2B1 into SGs. We further demonstrate that transient SG formation contributes to persistent accumulation of TDP-43 into cytoplasmic puncta and that our hit compounds can reduce this accumulation in iPS-MNs from ALS patients. We propose that compounds with planar moieties represent a promising starting point to develop small-molecule therapeutics for treating ALS/FTD.

INTRODUCTION

Stress granules (SGs) assemble transiently in response to cellular stress as an adaptive survival mechanism (Kedersha and Anderson, 2007; Kedersha et al., 2013). SGs contain proteins and mRNAs, which are translationally stalled via phosphorylation of serine 51 of the translation initiation factor eIF2 α (Kedersha and Anderson, 2007; Khong et al., 2017). By modulating translation and recruiting signaling proteins, SGs are believed to triage intracellular activity toward an integrated stress response (Arimoto et al., 2008; Harding et al., 2000; Sidrauski et al., 2015; Wippich et al., 2013). SGs are highly dynamic, exhibiting liquid-like behaviors and disassembling within minutes of removal of stress (Wheeler et al., 2016). These liquid-like properties are thought to be mediated by the intrinsically disordered regions (IDRs) common to many SG proteins (Alberti et al., 2009; Jain et al., 2016; Markmiller et al., 2018). Neurodegeneration-linked mutations in proteins such as FUS, HNRNPA2B1, and TDP-43 frequently cluster in the IDRs, potentially altering the liquid-like phase separation properties of these proteins (Chen-Plotkin et al., 2010; Ryan et al., 2018; Shang and Huang, 2016). These mutations are implicated in hereditary forms of frontotemporal dementia (FTD) and amyotrophic lateral sclerosis (ALS), fatal, incurable diseases characterized by progressive degeneration of cortical and motor neurons (Kim et al., 2013;

Sreedharan et al., 2008; Vance et al., 2009). *In vitro* studies of phase separated recombinant IDRs carrying ALS-associated mutations report that the mutations accelerate transition from a liquid-like state to a solid-like state (Kato et al., 2012; Kim et al., 2013; Patel et al., 2015; Ryan et al., 2018). To illustrate, recombinant mutant IDR from HNRNPA2B1 undergoes liquid-liquid phase separation followed by spontaneous maturation into insoluble fibers (Kim et al., 2013; Ryan et al., 2018). Therefore, these IDR mutations likely predispose assembly of inclusion bodies and are speculated to cause toxic loss and/or gain of function. Indeed, a hallmark feature of nearly all ALS patients is the presence of cytoplasmic TDP-43-containing inclusion bodies within MNs that contain SG-associated proteins (Bentmann et al., 2012; Blokhuis et al., 2013; Farg et al., 2013; Keller et al., 2012; Kim et al., 2013; Liu-Yesuevitz et al., 2010).

Recent studies of the composition of SGs have revealed that a large fraction of SG proteins extensively interact prior to stress (Markmiller et al., 2018). Also, a super-resolution microscopy study has reported the existence of substructures called SG cores, around which additional proteins and RNAs assemble into the SG shell (Jain et al., 2016). It is very likely that cores and shells contain different protein components, with differences that may relate to disease pathogenesis (Jain et al., 2016; Khong et al., 2017). Excitingly, modulation of some SG proteins appears to alleviate degenerative phenotypes in animal models of ALS (Becker et al., 2017; Kim et al., 2014; Markmiller et al., 2018). Despite these advances, there still exists an urgent need to understand how ALS-associated proteins such as TDP-43 relate to SGs and for new tools that can readily perturb these relationships.

Thus, to accelerate our understanding of SGs and their connections to neurodegenerative disease, we conducted a high-content screen (HCS) for small molecules that robustly modulate aspects of SG biology. We identified several classes of SG-modulating compounds, including small molecules that act at cell-surface targets such as ion channels, receptors, or lipid membranes and compounds that modulate inflammatory signaling pathways. Interestingly, one large group of structurally related molecules to emerge from the screen was characterized by the presence of planar aromatic side chains. Such planar moieties are characteristic of nucleic acid intercalating molecules, supporting the hypothesis that SG formation requires nucleic acid interactions. We discovered that SGs accumulate ALS-associated proteins in an RNA-dependent manner and that planar molecules disrupt this accumulation. We show that transient SG induction through puromycin treatment can induce persistent localization of TDP-43 into cytoplasmic puncta in human-induced pluripotent stem cell-derived MNs (iPS-MNs) carrying ALS-associated mutations in *TARDBP* or *FUS*. Excitingly, molecules with planar moieties prevented SG localization of TDP-43 and reduced accumulation of TDP-43 into persistent cytoplasmic puncta in mutant iPS-MNs. These results expand our understanding of SG biology, offer a molecular toolbox to study the mechanistic relationship between SGs and disease pathophysiology, and pave the way to developing a new class of therapeutics for ALS/FTD.

RESULTS

G3BP1-GFP Transgenic Cell Lines Enable Robust Image-Based SG Screening

G3BP1 is a key protein required for SG formation (Kedersha and Anderson, 2007; Kedersha et al., 2016). As G3BP1 is found in both the SG core and, to a lesser extent, the SG shell, we reasoned that identifying compounds that modulate G3BP1-positive puncta will unveil molecular principles of SG formation and mechanistic links between SGs and disease (Jain et al., 2016). We used CRISPR/Cas9 genome editing in HEK293xT cells and the human-induced pluripotent stem cell (hiPSC) line CV-B to fuse GFP to the C terminus of G3BP1 at the endogenous locus (Figures 1A and S1A) (Gore et al., 2011). CV-B hiPSCs were subsequently differentiated into neural precursor cells (NPCs) or MNs (iPS-MNs; Figures 1B, S1A, and S1B) (Reinhardt et al., 2013). Upon exposure to sodium arsenite (NaAsO_2) oxidative stress, these G3BP1-GFP cell lines robustly and reproducibly formed bright GFP-positive puncta, which co-localized with SG proteins UBAP2L, CAPRIN1, DDX3, and PABPC1, consistent with formation of G3BP1-containing SGs (Figures 1C and S1C). These G3BP1-GFP-positive SGs did not co-localize with negative control staining for cytochrome c (CYC), although as expected CYC staining detects filamentous structures resembling mitochondria (Figure S1C). These G3BP1-GFP-positive SGs were abrogated by pre-treatment with cycloheximide, as previously reported (Figure 1C) (Kedersha and Anderson, 2007). Our results indicate that these G3BP1-GFP reporter lines faithfully recapitulate SG dynamics.

We conducted the primary SG screen in the HEK293xT and NPC lines, as they can be expanded to large quantities. The screening strategy entailed first pre-treating cells with compounds before stressing with NaAsO_2 (Figure 1D). This order of operations is most likely to capture both compounds that prevent SG assembly as well as compounds that promote disassembly of SGs after they have begun to form. We next determined the Z' statistic, which describes the robustness of the signal-to-noise ratio of a screen assay: a Z' value of 0.5 indicates a statistical difference of 12 SDs between the positive and negative control samples, and Z' values close to or above 0.5 are desirable for a robust HCS assay (Zhang et al., 1999). We calculated Z' values of 0.51 and 0.42 for HEK293xT cells and NPCs, respectively, and concluded that the signal-to-noise ratio of the screen assay is sufficient for HCS (Figure 1E).

High-Content Screening Identifies Diverse Classes of SG-Modulating Compounds

We screened 3,350 and 5,910 compounds in biological duplicate in HEK293xT cells and NPCs, respectively (Figure 2A). The compounds were deliberately sourced from five complex small-molecule libraries spanning a wide range of chemical structures and biological activities. Cells were pre-treated with compounds, stressed, fixed, and imaged. Screen images were segmented to identify DAPI-stained nuclei and G3BP1-GFP-positive SGs. The amount of SG formation per cell was quantified as the total image area enclosed in SGs divided by the total image area enclosed in nuclei. Total nuclei area was a surrogate for number of nuclei due to limitations in automated

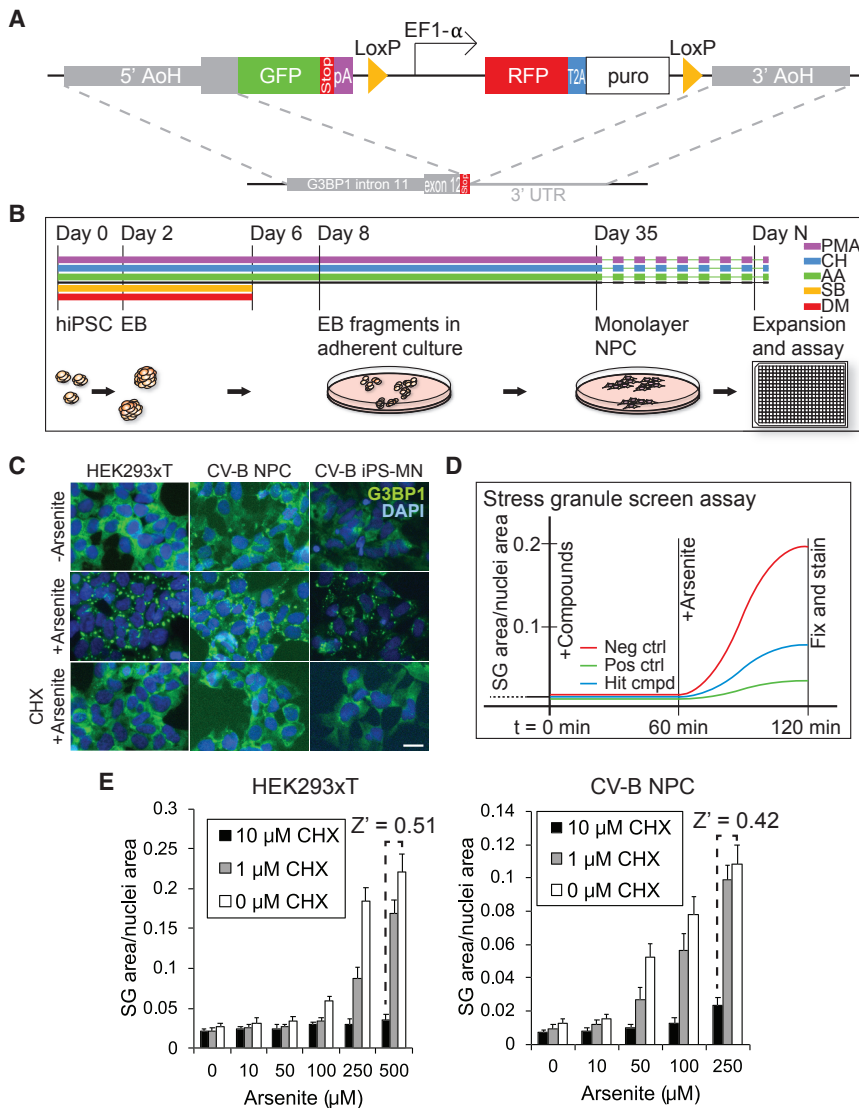


Figure 1. SG Reporter Lines Enable Robust Image-Based Screening

(A) GFP construct inserted in endogenous *G3BP1* locus. AoH, arm of homology.

(B) NPC differentiation from hiPSCs. EB, embryoid bodies; PMA, purmorphamine; CH, CHIR99021; AA, L-ascorbic acid; SB, SB431542; DM, dorso-morphin.

(C) Representative images of *G3BP1*-GFP SG reporter lines under no stress, NaAsO₂ stress (HEK293xT cells, NPCs, or iPS-MNs: 500/250/100 µM, 60 min) and NaAsO₂ stress plus CHX pre-treatment (10 µM, 60 min). n = 4 biological replicates. Scale bar is 50 µm. NaAsO₂, sodium arsenite; CHX, cycloheximide.

(D) Screening paradigm: cells were pre-treated with compounds (10 µM, 60 min) followed by NaAsO₂ stress (293T or NPC: 500/250 µM, 60 min).

(E) Quantification of SG area/nuclei area for varying concentrations of CHX pre-treatment (60 min) and NaAsO₂ stress (60 min). Z' for the screen assay: $Z' = 1 - \frac{(3(\hat{\sigma}_p + \hat{\sigma}_n)/|\hat{\mu}_p - \hat{\mu}_n|)}{|\hat{\mu}_p - \hat{\mu}_n|}$, where $\hat{\sigma}_p$ and $\hat{\sigma}_n$ are sample SDs and $\hat{\mu}_p$ and $\hat{\mu}_n$ are sample means for positive and negative controls. Bars are mean ± SD, n = 4 biological replicates.

See also Figure S1.

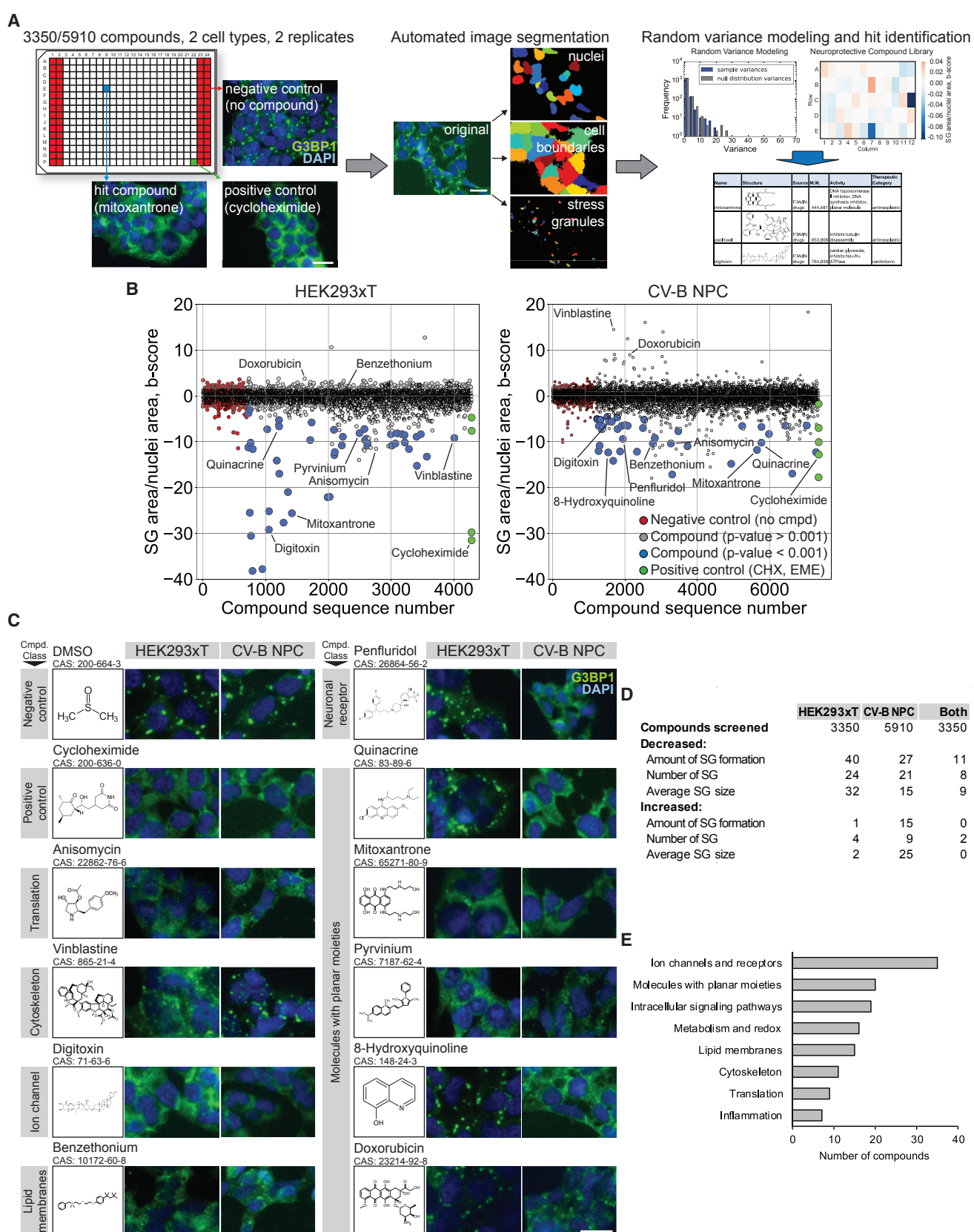
segmentation of nuclei located close together. We also reasoned that screen compounds may alter the average SG size and/or the number of SGs per cell, for example, by inhibiting assembly of SG shell proteins onto SG cores or by impairing SG fusion, leading to smaller but more numerous SGs. We therefore computed two further metrics: the number of SGs per cell quantified as the number of SG puncta divided by the total image area enclosed in nuclei, and the average SG size quantified as the total image area enclosed in SGs divided by the number of SG puncta.

In the first-pass analysis of the screen, we prioritized avoiding false negatives over accumulating false positives and eliminated the latter through manual examination of the screen raw images for imaging artifacts and confounding effects such as autofluorescence and cytotoxicity. We identified 40 and 27 compounds that reduced the amount of SG formation per cell in HEK293xT cells and NPCs, respectively (Figures 2B–2D and S2A). Additionally, we identified ~50 compounds that modulated SGs in other ways, such as increasing or

decreasing the average SG size or number of SGs per cell (Figures 2C, 2D, S2A, and S2B). Hit compounds were annotated by their reported cellular targets using the National Center for Biotechnology Information PubChem database (Figures 2E and S2A; Table S1). Supporting the validity of our screening approach, we confirmed that ribosomal inhibitors strongly reduced the amount of SG formation per cell, as previously reported (Figures 2C, 2E, and S2A; Tables S2, S3, and S4) (Kedersha and Anderson, 2007). These include anisomycin

and neomycin, which bind to the ribosomal A-site or induce errors in tRNA selection, respectively (Garreau de Loubresse et al., 2014; Prokhorova et al., 2017). Both positive controls, cycloheximide and emetine, bind to the ribosomal E-site and halt translocation (Schneider-Poetsch et al., 2010; Wong et al., 2014). We also confirmed that cytoskeleton targeting compounds, such as vincristine and vinblastine, which inhibit tubulin polymerization, the microtubule stabilizing drug paclitaxel, and the actin filament stabilizer prieurianin, altered average size and/or number of SGs per cell (Figures 2C, 2E, and S2A; Tables S2, S3, and S4). This is consistent with previous reports that the cytoskeleton and associated molecular motors play key roles in SG migration, fusion, and maturation (Ivanov et al., 2003).

Among our hit compounds that have not previously been reported to modulate SGs, we identified >30 that act on cell-surface targets, such as ion channels, receptors, transporters, and lipid membranes, targets which have not been previously



(legend on next page)

implicated in modulating SGs (Figures 2E and S2A; Table S1). We identified a large group of cardiac glycosides including digoxin and proscloradin A, which inhibit the Na^+/K^+ -ATPase (Figure 2C; Tables S2, S3, and S4). Intriguingly, cardiac glycosides were previously shown to disperse nuclear TDP-43 foci in ALS patient-derived iPS-MNs, though it remains unclear how these compounds exert this effect and whether these nuclear TDP-43 foci are related to SGs (Burkhardt et al., 2013). We also identified the receptor tyrosine kinase inhibitor tyrphostin A9, reported to increase the survival of MNs carrying SOD1 mutations (Tables S2, S3, and S4) (Yang et al., 2013). However, it is uncertain whether this survival effect is connected to SG modulation. Overall, one possibility is that these compounds modulate SGs by interfering with intracellular ion, solute, and/or osmolarity homeostasis. Physical-chemical properties such as tonicity, concentration of the divalent cation Zn^{2+} , and concentration of the hydrotrope ATP regulate phase transitions of proteins such as FUS and TIA1, which may be important for SG formation (Banani et al., 2017; Patel et al., 2017; Rayman et al., 2018).

We also identified >40 compounds that target a broad range of intracellular processes, including inflammatory molecule biosynthesis pathways (Figures 2E and S2A; Table S1). We identified seven compounds that have anti-inflammatory activities, including quinacrine, an inhibitor of phospholipase A2 (PLA2), and oxyphenbutazone, a cyclooxygenase inhibitor (Figure 2C; Tables S2, S3, and S4). Two hit compounds target DYRK and RACK1 proteins at the intersection of SGs and mTOR signaling and SGs and SAPK signaling, respectively (Tables S2, S3, and S4) (Arimoto et al., 2008; Wippich et al., 2013). The screen also revealed compounds that modulate metabolic processes regulating SGs, including autophagosomes, proteasomes, and heat shock proteins (Tables S2, S3, and S4) (Buchan et al., 2013; Turakhia et al., 2018).

Strikingly, we identified a large group of ~20 SG-modulatory compounds that contain extended planar moieties, many of which act as nucleic acid intercalating molecules, including mitoxantrone, quinacrine, doxorubicin, and daunorubicin (Figures 2C, 2E, and S2A; Tables S1, S2, S3, and S4). Planar molecules have not previously been reported to modulate SGs, but these compounds strongly altered the amount, the average size, and the number of SGs per cell (Figure S2A; Tables S2, S3, and S4). Notably, doxorubicin has recently been shown to change the phase transition diagram of RNA-only condensates containing CAG or CUG repeats *in vitro* and *in vivo* (Jain and Vale, 2017; Khong et al., 2017). Furthermore, quinacrine, another planar molecule, has been reported to directly bind to the prion-like

domain of prion protein PrP and inhibit aggregation *in vitro* (Korth et al., 2001).

To verify that these planar molecules are not false positives intercalating into nuclear DNA and altering nuclei area rather than SG area, we examined the nuclei area of cells treated with planar compounds, as well as representative compounds from the other hit compound classes. The hit compounds did not alter nuclei area compared to DMSO (Figure S2C). Instead, we hypothesized that these planar compounds modulate SGs by interacting with RNAs or protein IDRs contained therein.

Hit Compounds Robustly Inhibit SG Formation across Different Stress Contexts

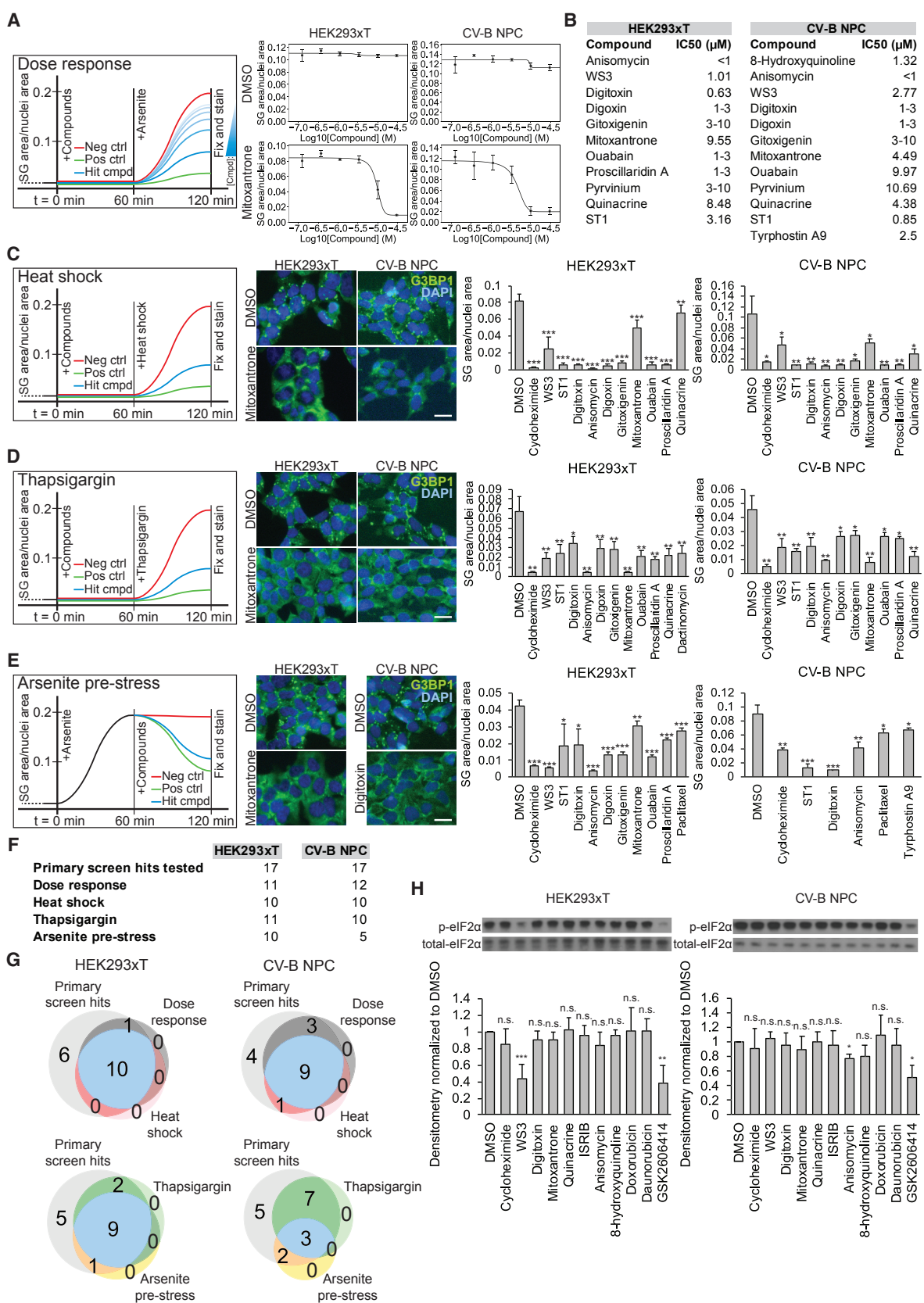
We selected 17 compounds for further study in counterscreens, focusing on the two most highly represented groups of hit compounds: planar molecules and cardiac glycosides (Table S5). First, we found that in HEK293xTs and NPCs, 11 and 12 compounds, respectively, inhibited SG formation in a dose-dependent manner over a concentration range spanning three orders of magnitude and covering the initial screen concentration of 10 μM (Figures 3A and S3A). The remaining 6 and 5 compounds neither decreased nor increased SG formation with increasing compound concentration. We estimated the compounds' 50% inhibitory concentrations (IC_{50} s) from fitted logistic functions (Figure 3B). All but one of the IC_{50} s were in the single-digit micromolar range, a common starting potency for further optimization (Teague et al., 1999). In particular, we hypothesized that the planar compounds bind to RNA and/or SG protein IDRs, which are relatively unstructured and often lack small-molecule binding pockets, leading to IC_{50} s in the micromolar range (Guan and Disney, 2012; Stelzer et al., 2011; Warner et al., 2018).

We next showed that in both HEK293xT cells and NPCs, ≥ 10 compounds significantly inhibited SG formation under heat shock unfolded-protein stress or thapsigargin poisoning of the autophagosome, which hinders SG clearance by autophagy (Figures 3C and 3D) (Buchan et al., 2013). These findings suggest that the hit compounds do not act in ways specific to any particular stressor (e.g., scavenging NaAsO_2 -induced free radicals) but rather via mechanisms downstream of where orthogonal stress pathways converge to induce SG formation.

We found 10 and 5 compounds in HEK293xT cells and NPCs, respectively, which significantly disassembled pre-formed SGs when added after SGs had already formed in response to NaAsO_2 stress (Figure 3E). This confirms that our compound-first, stress-second screening paradigm successfully identified not only compounds that prevent SG formation but also

Figure 2. High-Content Screening Identifies Diverse Classes of SG-Modulating Compounds

- (A) Experimental and computational pipeline for screen. Scale bars are 50 μm .
- (B) Scatter plots of amount of SG formation (SG area/nuclei area) for screen. Means of two to four biological duplicate b-scores are represented. Red points: negative controls (no compound). Green points: positive controls (CHX or EME). Blue points: compounds which significantly reduced amount of SG formation ($p < 0.001$, modified one-sample t tests). EME, emetine.
- (C) Left: screen hit compounds, skeletal formulae, and compound classifications by the reported cellular targets in the National Center for Biotechnology Information (NCBI) PubChem database. Right: representative images from screen. $n \geq 2$ biological replicates. Scale bar is 50 μm .
- (D) Numbers of SG-modulating compounds. Amount of SG formation = SG area/nuclei area. Number of SG = SG count/nuclei area. Average SG size = SG area/SG count.
- (E) Classification of hit compounds by their reported cellular targets in the NCBI PubChem database.
See also Figure S2 and Tables S1, S2, S3, and S4.



(legend on next page)

compounds that induce disassembly of SGs after they have begun to form. In summary, the compounds tested in the counterscreens, most of which are planar molecules or cardiac glycosides, robustly inhibited SGs across diverse stress contexts (Figures 3F and 3G and Figure S4A). Last, we showed that seven of 13 compounds tested, five of which are planar, also reduced assembly of Rasputin-positive puncta in NaAsO₂-stressed S2 cells. Rasputin is the *Drosophila melanogaster* ortholog of G3BP1. These data indicate that the mechanism of action of planar compounds on SGs is conserved across species.

Hit Compounds Inhibit SG Formation Independently of eIF2 α Phosphorylation and Translational Arrest

Seeking to further characterize mechanisms of action, we were surprised to find that seven of eight hit compounds tested (five are planar compounds) did not alter NaAsO₂-induced phosphorylation of eIF2 α at serine 51 or total eIF2 α levels (Figures 3H and S4B). As previously reported, the selective PERK inhibitor GSK2606414 significantly reduced eIF2 α phosphorylation (Figures 3H and S4B) (Kim et al., 2014). Interestingly, in the absence of stress the EBP1 kinase targeting compound WS3, as well as digitoxin, anisomycin, the antimicrobial 8-hydroxyquinoline, and GSK2606414 significantly increased eIF2 α phosphorylation above baseline without inducing SG formation (Figures S4C–S4E).

Further, 10 of 10 hit compounds tested (seven are planar compounds) could modulate SG formation without reversing stress-induced translational arrest in HEK293xT cells, as determined by puromycin incorporation into nascent polypeptides (SUNSET assay, Figure S4F) (Schmidt et al., 2009). Unexpectedly, GSK2606414 did not reverse stress-induced translational arrest despite decreasing eIF2 α phosphorylation (Figures 3H and S4F). Although we found the eIF2B agonist integrated stress response inhibitor (ISRB1) did not reverse gross translational arrest, the compound has been reported to modulate translation of specific stress-response proteins during cellular stress (Figure S4F) (Sidrauski et al., 2015; Zryanova et al., 2018). Overall, these results indicate that our hit compounds (excepting WS3) can decouple eIF2 α phosphorylation and translational arrest from SG formation. Instead, these compounds likely act on SGs themselves rather than on upstream eIF2 α kinases or translation.

Hit Compounds Inhibit SG Formation in iPS-MNs

As the primary and counterscreens were performed in proliferative cells, we next evaluated whether the hit compounds inhibit SG formation in post-mitotic iPS-MNs. We concurrently generated iPS-MNs from four hiPSC lines derived from four individuals carrying ALS-linked mutations in the C-terminal IDR of TDP-43 (N352S and G298S), two hiPSC lines from two individuals harboring mutations in the C-terminal nuclear localization signal (NLS) of FUS (R521G), and four control hiPSC lines from three healthy individuals who are genetically related to the individuals carrying ALS-associated mutations (Figure S5A; Table S6). We selected 10 hit compounds that are representative of the hit compound classes and were validated in counterscreens, including five planar molecules (Table S7).

We induced SGs in iPS-MNs using NaAsO₂, thapsigargin, and puromycin, the last of which leads to robust SGs in post-mitotic neurons (Kedersha and Anderson, 2007; Markmiller et al., 2018; Martinez et al., 2016; Turakhya et al., 2018). We observed that the compounds inhibited SG formation across all lines, regardless of mutation status (Figures 4A–4C). Six of 10 compounds, including the three planar molecules quinacrine, mitoxantrone, and pyrinium, strongly reduced SG formation in all three stress contexts (Figures 4A–4C). The remaining four compounds, including the two planar molecules 8-hydroxyquinoline and daunorubicin, reduced SG formation in two of three stress contexts (Figures 4A–4C). We concluded that our hit compounds are able to recapitulate SG inhibition in patient-derived iPS-MNs.

ALS-Associated RNA-Binding Proteins Are Recruited to SGs

Contemporaneous with the SG screen, we utilized the G3BP1-GFP reporter lines to characterize molecular mechanisms by which ALS-associated RNA-binding proteins (RBPs) such as TDP-43, FUS, HNRNPA2B1, and TIA1 are recruited to SGs. To determine whether these proteins are preferentially recruited to one of the recently reported SG subcompartments (i.e., core versus shell), we used a previously described protocol to isolate SG-enriched fractions from G3BP1-GFP expressing cells (Jain et al., 2016). As expected, we found that fractions isolated from NaAsO₂-stressed cells contained compact GFP-positive bodies, whereas those from unstressed cells showed diffuse GFP signal (Figure 5A). Gel electrophoresis and subsequent

Figure 3. Hit Compounds Robustly Inhibit SGs across Multiple Stress Contexts

(A) Left: assay for dose-dependent inhibition of NaAsO₂-induced SG formation (293T or NPC: 500/250 μ M, 60 min). Right: scatter plots and logistic regressions of dose-dependent reduction of SG area/nuclei area by pre-treatment with mitoxantrone (0.12–30 μ M, 60 min) or DMSO. Points are mean \pm SD, n = 4 biological replicates.

(B) IC₅₀s for SG inhibiting compounds, estimated from midpoints of logistic curves fitted by least-squares regression.

(C–E) Left: assay for inhibiting SG formation under heat shock stress (C; 43°C, 60 min) or thapsigargin stress (D; 293T or NPC: 50/1 μ M, 60 min) or reversing NaAsO₂-induced SG formation (E; 293T or NPC: 250/100 μ M, 60 min). Center: representative images of cells treated with DMSO, mitoxantrone, or digitoxin (10 μ M, 60 min) followed by heat shock stress (C) or thapsigargin stress (D) or after cells had been pre-stressed with NaAsO₂ (E). Scale bars are 50 μ m. Right: quantification of SG area/nuclei area in cells treated with hit compounds (10 μ M, 60 min) followed by heat shock stress (C) or thapsigargin stress (D) or after cells had been pre-stressed with NaAsO₂ (E). *p < 0.05, **p < 0.01, ***p < 0.001, two-sample t tests to DMSO. Bars are mean \pm SD, n = 4 biological replicates.

(F) Numbers of compounds which reduced SG area/nuclei area in counterscreens.

(G) Venn diagrams showing numbers of compounds that reduced SG area/nuclei area in one or more counterscreens.

(H) Top: representative blots of phosphorylated versus total eIF2 α in cells pre-treated with hit compounds (10 μ M, 60 min) and stressed with NaAsO₂ (293T or NPC: 500 μ M, 40 min/250 μ M, 60 min). Bottom: quantification of blots of phosphorylated eIF2 α , as in (H, top panel). *p < 0.05, **p < 0.01, ***p < 0.001, one-sample t tests. Bars are mean \pm SD, n = 3 experimental replicates.

See also Figures S3 and S4 and Table S5.

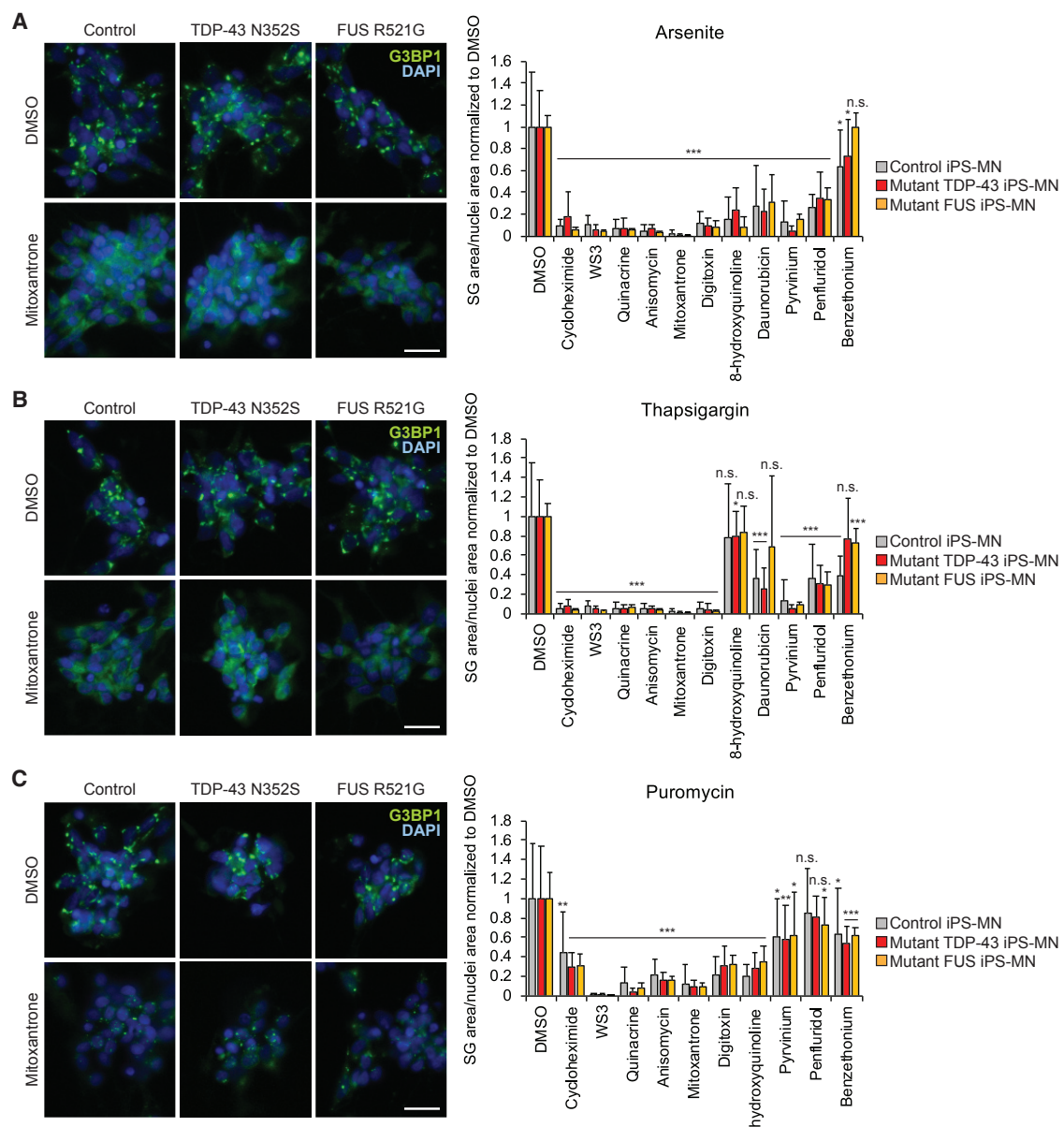


Figure 4. Hit Compounds Inhibit SG Formation in iPS-MNs

(A–C) Left: representative immunofluorescence (IF) images of iPS-MNs pre-treated with mitoxantrone (10 µM, 80 min) or DMSO and stressed with NaAsO₂ (A; 100 µM, 120 min) or thapsigargin (B; 250 nM, 120 min) or treated with mitoxantrone + puromycin (C; 5 µM + 5 µg/mL, 12 h). Scale bars are 20 µm. Right: quantification of SG area/nuclei area of iPS-MNs pre-treated with screen compounds (10 µM, 80 min) and stressed with NaAsO₂ (A) or thapsigargin (B) or treated with screen compounds + puromycin (C; 5 µM + 5 µg/mL, 12 h). *p < 0.05, **p < 0.01, ***p < 0.001, two-sample t tests to DMSO. Bars are mean ± SD, n ≥ 5 biological replicates of each of four control, four TARDP mutant and two FUS mutant lines.

See also Figure S5 and Tables S6 and S7.

silver staining of fractions from stressed versus unstressed cells revealed changes in band intensities for numerous proteins upon NaAsO₂ stress, likely representing increased levels of SG shell proteins and proportionally decreased levels of SG core proteins as SG composition becomes more complex (Figure 5B).

Surprisingly, when we performed western blot analysis of fractions from stressed versus unstressed cells, we found that the relative abundances of well-known SG proteins decreased

upon NaAsO₂ stress, whereas the relative abundances of four ALS-associated proteins increased (Figures 5C and 5D). Supporting and extending recent proximity-labeling proteomic studies of SGs, our western blot results indicate that well-known SG proteins already pre-exist in a core-like complex with G3BP1 even in the absence of stress, while other proteins assemble onto SGs specifically during stress, potentially forming the SG shell (Markmiller et al., 2018).

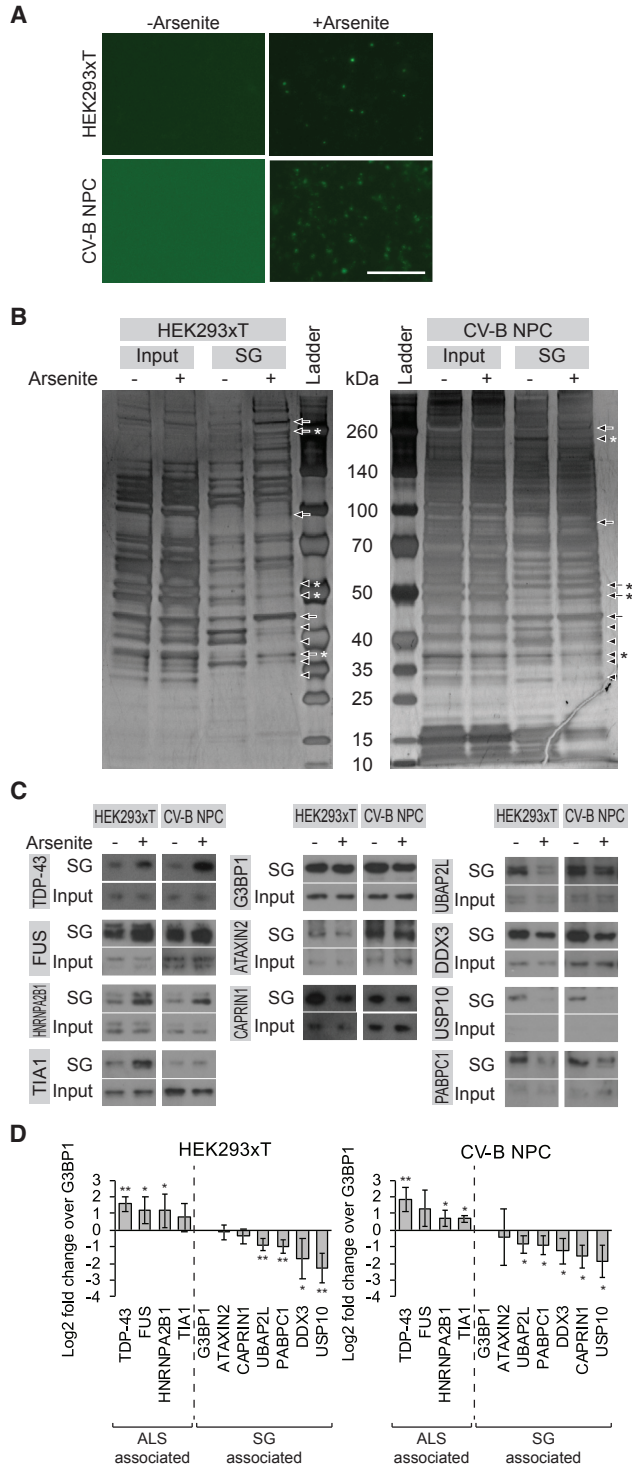


Figure 5. ALS-Associated RBPs Are Recruited into SGs

(A–C) Representative images (A), silver stains (B), and western blots (C) of SG-enriched fractions from unstressed versus NaAsO₂ stressed (293T or NPC; 500/250 μM, 60 min) cells. Arrows: bands stronger in fractions from stressed cells. Arrowheads: bands fainter in fractions from stressed cells. Stars: cell-type specific differences in band intensity changes. n = 3 experimental replicates. Scale bar is 20 μm.

Recruitment of ALS-Associated RBPs into SGs Is RNA Dependent

SGs are highly enriched in RBPs and it is well known that RNA binding can mediate a significant fraction of interactions among RBPs, including TDP-43 (Bentmann et al., 2012; Brannan et al., 2016). However, it has not been determined to what degree RBP-RNA interactions are essential for SG recruitment of most SG and ALS-associated proteins. We found by western blotting that RNase I digestion of SG-enriched fractions from NaAsO₂-stressed cells reduced the association of HNRNPA2B1 with SGs in a dose-dependent manner (Figures S6A and S6B). We found similar results for TDP-43 and FUS, while the SG association of UBAP2L and CAPRIN1 was resistant to RNase I digestion (Figures S6A and S6B).

We confirmed these results with immunofluorescence (IF) staining of SG-enriched fractions. For fractions from HEK293xT cells, co-localization of FUS and HNRNPA2B1, but not UBAP2L, with G3BP1-GFP-positive SGs decreased in a dose-dependent manner following RNase I digestion (Figures S6C–S6E). For fractions from NPCs, co-localization of HNRNPA2B1 with G3BP1-GFP-positive SGs decreased following RNase I digestion (Figures S6C–S6E). We additionally found that RNase I digestion only modestly decreased the average SG size or total amount of SGs in SG-enriched fractions (Figures S6F–S6H). This is consistent with previous reports that SGs are largely resistant to RNase I digestion and indicates that the reduction of TDP-43, FUS, and HNRNPA2B1 in SGs following RNase I digestion is not simply due to extensive breakdown of SGs (Jain et al., 2016). Rather, the western blot and IF results suggest that SG recruitment of HNRNPA2B1, and to a lesser extent TDP-43 and FUS, is RNA dependent. This corroborates recent reports that HNRNPA2B1 interacts with a large host of RBPs and ribonucleoparticles (RNPs) through RNA-dependent interactions, and that the RNA recognition motif (RRM) domain is required for TDP-43 recruitment to SGs (Bentmann et al., 2012; Brannan et al., 2016).

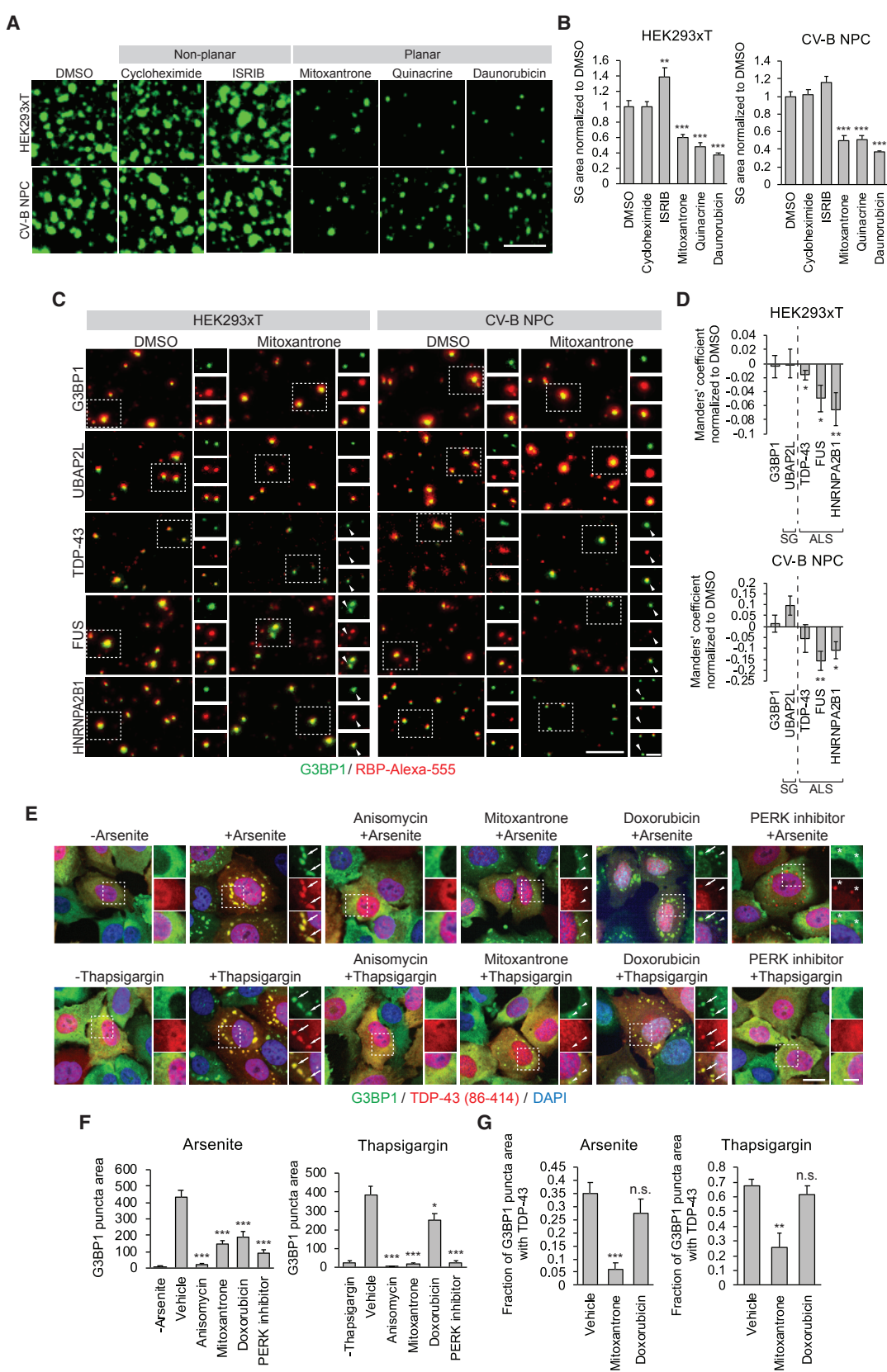
Molecules with Planar Moieties Reduce ALS-Associated RBPs from SGs

As described above, planar compounds decreased the average SG size while in some cases increasing the number of SGs per cell (Figure S2A). Planar SG-inhibiting compounds such as mitoxantrone, daunorubicin, quinacrine, and pyrvinium have been reported to be nucleic acid intercalating molecules that can directly bind to RNA (Ren and Chaires, 1999; Shen et al., 2013; Wang et al., 2013; Wilson et al., 1993; Zheng et al., 2009). We therefore reasoned that they might modulate SG growth and/or fusion by interfering with the RNA-dependent assembly of a set of RBPs onto SGs (Wheeler et al., 2016).

Indeed, western blot analysis of SG-enriched fractions incubated with mitoxantrone and daunorubicin indicated reduction of TDP-43 from SGs (Figure S7A). Additionally, three

(D) Quantification of blots as in (C). SG band intensities are divided by input band intensities, normalized to G3BP1, and log₂-transformed. *p < 0.05, **p < 0.01, one-sample t tests. Bars are mean ± SD, n = 3 experimental replicates.

See also Figure S6.



(legend on next page)

planar compounds, daunorubicin, pyrvium, and pararosaniline, reduced FUS and HNRNPA2B1 from SGs in fractions from HEK293xT cells and reduced TDP-43 and HNRNPA2B1 from SGs in fractions from NPCs (Figure S7A). By contrast, these planar compounds did not reduce G3BP1 or CAPRIN1 from SGs (Figure S7A).

On examination by fluorescence microscopy, we found that incubating SG-enriched fractions with mitoxantrone, quinacrine, and daunorubicin decreased the average size and total amount of G3BP1-GFP-positive SGs in the fractions, while the non-planar SG inhibiting compounds cycloheximide and ISRIB did not (Figures 6A, 6B, and S7B). ISRIB even appeared to stabilize SGs compared to DMSO (Figures 6A and 6B). This planar molecule-induced breakdown of SGs *in vitro*, possibly into SG core-like subcomplexes smaller than the resolution limit of fluorescence microscopy, is consistent with our hypothesis that these planar compounds exert their SG inhibitory effects directly on SGs themselves (Jain et al., 2016).

Crucially, IF analysis of SG-enriched fractions incubated with planar compounds corroborated the western blot data. SG-enriched fractions incubated with mitoxantrone demonstrated a significant decrease in co-localization of TDP-43, FUS, and HNRNPA2B1, but not UBAP2L, with G3BP1-GFP-positive SGs (Figures 6C and 6D). Similar findings were observed with quinacrine (Figure S7C). In contrast, the non-planar SG inhibiting compound ISRIB did not reduce co-localization of TDP-43, FUS, and HNRNPA2B1 with G3BP1-GFP-positive SGs (Figure S7D). The decrease in amount of G3BP1-GFP-positive SGs following incubation with mitoxantrone or quinacrine, observed in (Figure 6A), is not as readily apparent in the images in (Figure 6C). This is because the SG-enriched fractions were diluted 10-fold to facilitate co-localization analysis and because we selected image areas focused on residual SGs. As a control, when we stained SG-enriched fractions with DAPI, we found no co-localization between DAPI-stained DNA and IF stained G3BP1, UBAP2L, TDP-43, FUS, and HNRNPA2B1 (Figure S7E). This suggests that intercalation of planar molecules into DNA likely does not account for the decreased co-localization of TDP-43, FUS, and HNRNPA2B1 with SGs.

The western blot and IF results showing that association of G3BP1, UBAP2L, and CAPRIN1 in SGs is highly resistant to incubation with planar compounds is consistent with previous reports that well-known SG proteins robustly associate in a pre-existing core-like complex (Markmiller et al., 2018). On the other hand, the reduction of ALS-associated RBPs from SGs and decrease in the total amount of visible SGs support our hypothesis that planar compounds interfere with assembly of a set of RBPs onto SGs, which may be important for SG growth and/or fusion (Wheeler et al., 2016).

Mitoxantrone Inhibits TDP-43 Accumulation in SGs in Cells Expressing TDP-43 Δ NLS

Since compounds with planar moieties reduce TDP-43 from SGs *in vitro*, we next evaluated these compounds in disease-relevant cell models that harbor mislocalized TDP-43 protein. In H4 neuroglioma cells expressing G3BP1-mCherry and GFP-TDP-43 Δ NLS (86–414), NaAsO₂ or thapsigargin stress strongly induced formation of co-localized G3BP1-mCherry SGs and GFP-TDP-43 Δ NLS puncta (Figures 6E, 6F, and S7F).

As expected, the SG inhibiting compounds anisomycin, mitoxantrone, or the PERK inhibitor GSK2656157 significantly reduced the amount of G3BP1-mCherry SG formation per cell (Figures 6E and 6F). Excitingly, the planar compound mitoxantrone also strongly inhibited co-localization of GFP-TDP-43 Δ NLS and residual SGs, with retention of a strong fluorescent TDP-43 signal in the nucleus (Figures 6E, 6G, and S7G). By contrast, the non-planar compound GSK2656157 inhibited SG formation but left cytoplasmic GFP-TDP-43 Δ NLS puncta, which did not co-localize with G3BP1-mCherry (Figures 6E, 6F, and S7F). Interestingly, in this model system doxorubicin, which also contains planar moieties, reduced the amount of SG formation per cell but did not significantly reduce co-localization of GFP-TDP-43 Δ NLS with residual SGs (Figures 6E–6G). This is distinct from its action in HEK293xT cells and NPCs, in which doxorubicin did not reduce the amount of SG formation per cell but rather decreased the average SG size and increased the number of SGs per cell (Tables S2, S3, and S4). Doxorubicin thus appears to have differing effects on SGs depending on the cell type and exogenous expression of GFP-TDP-43 Δ NLS (86–414).

Figure 6. Molecules with Planar Moieties Reduce ALS-Associated RBPs from SGs

(A and B) Representative images (A) and quantification of total SG area (B) of NaAsO₂-induced, G3BP1-GFP-positive SG-enriched fractions incubated with SG inhibiting compounds (100 μ M, 4°C, overnight) versus DMSO. **p < 0.01, ***p < 0.001, two-sample t tests to DMSO. Bars are mean \pm SEM, n = 45 images from 3 experimental replicates. Scale bar is 10 μ m.

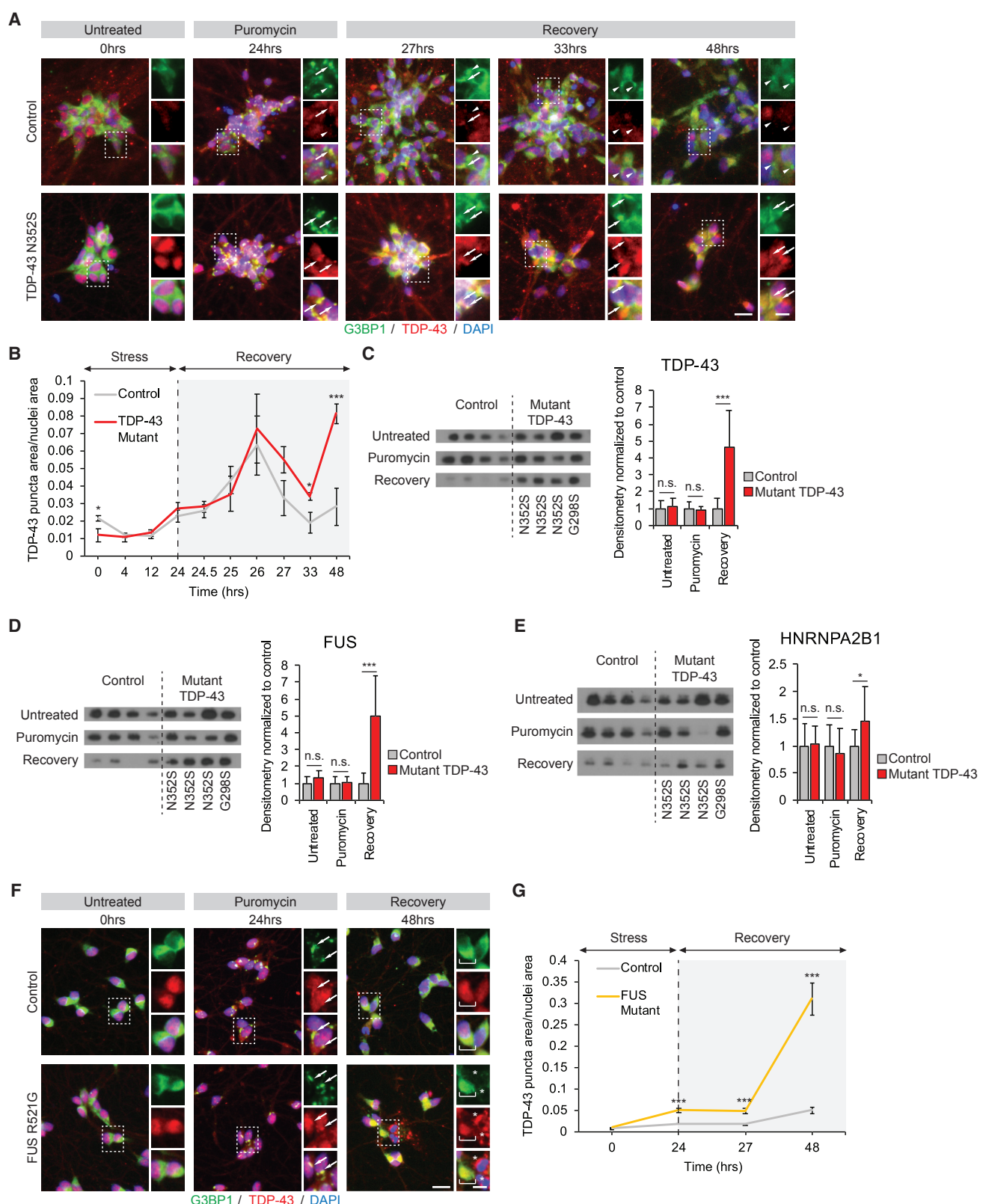
(C and D) Representative IF images (C) and quantifying change in Manders' correlation coefficient of co-localization between G3BP1-GFP and IF-stained RBPs (D) of NaAsO₂-induced (293T or NPC: 500/250 μ M, 60 min) SG-enriched fractions incubated with mitoxantrone (100 μ M, 4°C, overnight) versus DMSO. Arrowheads: G3BP1-GFP-positive SGs with reduced IF staining of RBPs. G3BP1 staining serves as IF staining control. *p < 0.05, **p < 0.01, one-sample t tests. Bars are mean \pm SEM, n = 45 images from 3 experimental replicates. Scale bar is 10 μ m (5 μ m for inset). RBP, RNA-binding protein.

(E) Representative images of H4 cells expressing exogenous G3BP1-mCherry (false-colored green for consistency) and doxycycline-inducible GFP-TDP-43 Δ NLS (residues 86–414; false-colored red). Cells were pre-treated with hit compounds (5 μ M, 30 min) and stressed with NaAsO₂ or thapsigargin (500 or 5 μ M, 60 min). Arrows: co-localized G3BP1-mCherry and GFP-TDP-43 Δ NLS puncta. Arrowheads: G3BP1-mCherry-only puncta. Stars: GFP-TDP-43 Δ NLS-only puncta. n \geq 14 cells. Scale bar is 50 μ m (20 μ m for inset). NLS, nuclear localization signal.

(F) Quantification of total G3BP1-mCherry puncta area, as in images in (E). *p < 0.05, ***p < 0.001, two-sample t tests to DMSO. Bars are mean \pm SEM, n \geq 35 cells.

(G) Quantification of the fraction of G3BP1-mCherry puncta area that has co-localized GFP-TDP-43 Δ NLS, as in images in (E). **p < 0.01, ***p < 0.001, two-sample t tests to DMSO. Bars are mean \pm SEM, n \geq 14 cells.

See also Figure S7.



(legend on next page)

In summary, these results suggest that some planar compounds (e.g., mitoxantrone) can inhibit accumulation of TDP-43 in SGs in live cells, while others (e.g., doxorubicin) cannot, possibly due to specific structural and chemical differences that prevent doxorubicin from binding to GFP-TDP-43 Δ NLS (86–414) in the same way as mitoxantrone in this model system.

Planar Compounds Reduce Persistent Cytoplasmic TDP-43 Puncta in Puromycin-Stressed iPS-MNs

Next, we evaluated whether compounds with planar moieties can mitigate ALS-associated molecular phenotypes. First, we determined whether SG formation leads to persistent accumulation of TDP-43 into cytoplasmic puncta in MNs, as has been reported for HeLa cells (Parker et al., 2012; Zhang et al., 2018). As before, we concurrently differentiated four control iPS-MN lines, four *TARDBP* mutant iPS-MN lines, and two *FUS* mutant iPS-MN lines. We stressed *TARDBP* mutant and control iPS-MNs with puromycin for 24 h, followed by washout and recovery from stress for 24 h. We found that during stress TDP-43 accumulated in SGs, and during recovery following washout of puromycin significantly more TDP-43 remained localized as cytoplasmic puncta (often with co-localized G3BP1) in the *TARDBP* mutants than in the controls (Figures 7A and 7B). Furthermore, SG-enriched fractions from *TARDBP* mutant iPS-MNs contained significantly more TDP-43, FUS, and G3BP1 (and to a lesser extent HNRNPA2B1 and CAPRIN1) than fractions from control iPS-MNs during recovery following stress (Figures 7C–7E, S8A, and S8B). These results were despite similar SG assembly and dissolution dynamics (Figure S8C). To control for potential confounding effects due to the sex of these iPS-MN lines, given that ALS is more common in males, we compared the amounts of cytoplasmic TDP-43 puncta between female and male iPS-MNs and found no significant differences (Figure S8D) (McCombe and Henderson, 2010). Strikingly, iPS-MNs harboring ALS-associated *FUS* mutations also showed a dramatic increase in cytoplasmic TDP-43 puncta compared to controls (Figures 7F and 7G). This manifested in roughly 10%–20% of cells as large cytoplasmic TDP-43 puncta that did not co-localize with G3BP1 (Figure 7F).

Encouraged that iPS-MNs carrying ALS-associated mutations exhibit a clear molecular phenotype, we next incubated control, *TARDBP* mutant, and *FUS* mutant iPS-MNs with DMSO, cycloheximide, or mitoxantrone during puromycin stress. Both cycloheximide and mitoxantrone strongly inhibited SG formation

(Figure 4C). However, as expected only mitoxantrone significantly abrogated cytoplasmic TDP-43 puncta in both control and *TARDBP* mutant iPS-MNs (Figures 8A and 8B). Furthermore, both mitoxantrone and pyrvium, another planar compound, produced lasting reductions of cytoplasmic TDP-43 puncta in *TARDBP* mutant iPS-MNs and to a lesser extent in *FUS* mutant and control iPS-MNs: these reductions extended at least 7 h into stress recovery after puromycin washout (Figures 8C, 8D, and S8E–S8H). By contrast, digitoxin, a non-planar SG-inhibiting compound, did not reduce cytoplasmic TDP-43 puncta (Figures 8C, 8D, and S8E–S8H). These results indicate that planar molecules can prevent the ALS-associated phenotype of persistent cytoplasmic TDP-43 puncta. Crucially, these compounds decreased the amount of cytoplasmic TDP-43 puncta in puromycin-stressed *TARDBP* mutant iPS-MNs to levels observed in unstressed control iPS-MNs (Figures 8C and S8E).

Finally, we tested planar compounds in mouse primary neurons expressing TDP-43(M337V)-EGFP, which exhibit TDP-43 mislocalized into cytoplasmic foci and higher cumulative death rates than control neurons expressing EGFP (Barmada et al., 2010). Excitingly, two planar compounds, mitoxantrone and doxorubicin, significantly reduced the cumulative death rate to levels comparable to the control neurons (Figure S8I). These data indicate that planar compound reduction of persistent cytoplasmic TDP-43 foci in iPS-MNs correlates with improved survival of neurons expressing mutant TDP-43 protein.

DISCUSSION

Previous studies of SGs in disease models have relied on a handful of SG modulators: cycloheximide, PERK inhibitors, or ISRIB. Here, we performed a screen identifying ~100 compounds representing eight compound classes that modulate SG formation. This diversity of SG-modulating compounds greatly expands the toolbox of molecules with which to probe the relationship between SGs and disease.

This study is also the first high-content screen for compounds that modulate not only the overall amount of SG formation but also SG size and numbers of SGs per cell. One class of compounds—the planar molecules—emerged as modulators of SG size and number. These compounds may help reveal the molecular rules underlying SG shell formation, SG fusion, and maturation. Interestingly, we found that seven compounds (five planar molecules) modulated SG formation without altering phosphorylation of eIF2 α . We also determined that 10

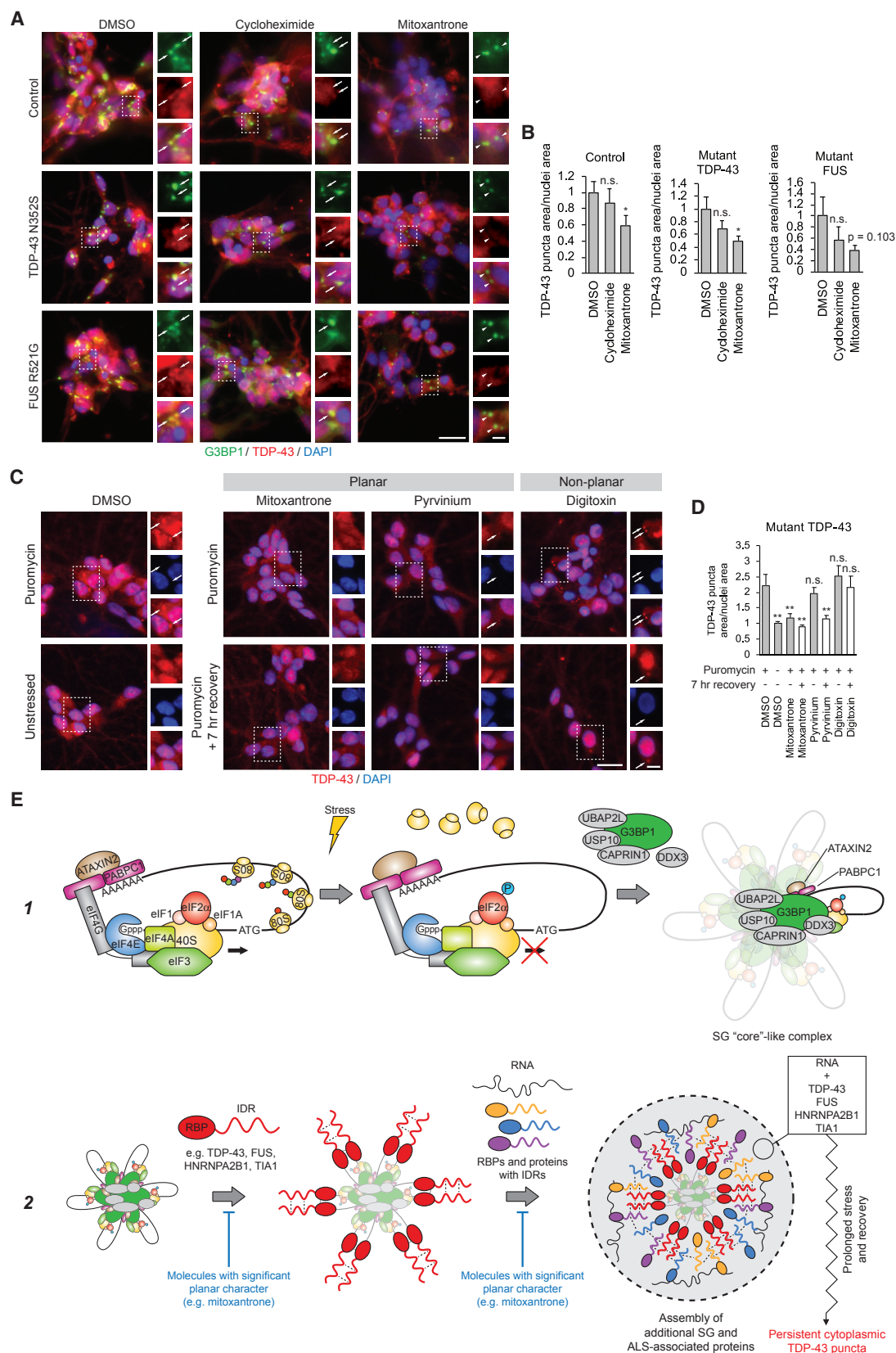
Figure 7. Puromycin-Stressed Mutant iPS-MNs Exhibit Persistent Cytoplasmic TDP-43 Puncta

(A and B) Representative IF images (A) and quantification of cytoplasmic TDP-43 puncta area/nuclei area (B) of iPS-MNs during puromycin stress (5 μ g/mL, 24 h) and recovery following puromycin washout (24 h). Arrows: cytoplasmic TDP-43 and G3BP1 puncta. Arrowheads: G3BP1-only puncta. *p < 0.05, ***p < 0.001, two-sample t tests to control iPS-MNs. Points are mean \pm SEM, n \geq 5 biological replicates of each of four control and four *TARDBP* mutant lines. Scale bar is 20 μ m (10 μ m for inset).

(C–E) Left: representative blots of TDP-43 (C), FUS (D), or HNRNPA2B1 (E) in SG-enriched fractions from iPS-MNs under no stress, puromycin stress (5 μ g/mL, 24 h), or puromycin stress plus 24 h recovery following puromycin washout. Right: quantification of blots as in (C)–(E) (left panel). *p < 0.05, ***p < 0.001, two-sample t tests to control iPS-MNs. Bars are mean \pm SD, n = 3 biological replicates of each of four control and four *TARDBP* mutant lines.

(F and G) Representative IF images (F) and quantification of cytoplasmic TDP-43 puncta area/nuclei area (G) of iPS-MNs during puromycin stress (5 μ g/mL, 24 h) and recovery following puromycin washout (24 h). Arrows: cytoplasmic TDP-43 and G3BP1 puncta. Brackets: broad regions of cytoplasmic TDP-43. Stars: TDP-43-only puncta. ***p < 0.001, two-sample t tests to control iPS-MNs. Points are mean \pm SEM, n \geq 5 biological replicates of each of four control and two *FUS* mutant lines. Scale bar is 20 μ m (10 μ m for inset).

See also Figure S8.



(legend on next page)

compounds (seven planar molecules) modulated SG formation without reversing stress-induced translational arrest. This study therefore also offers SG-inhibiting compounds that act through orthogonal mechanisms, which will be useful in dissecting the molecular details of SG formation.

To evaluate how compounds affect specific subcompartments of SGs such as cores versus shells, we leveraged a recently published biochemical approach to isolate SG-enriched fractions (Jain et al., 2016). In these fractions, we found that the relative representation of certain SG proteins, which may exist as pre-formed core-like complexes, is reduced upon stress due to assembly of a complex array of additional proteins onto SGs (Markmiller et al., 2018). These additional proteins, which may contribute toward formation of SG shells, include ALS-associated proteins, whose assembly onto SGs is sensitive to RNase I. Moreover, we found that planar compounds that have been reported to interact with RNA also dislodged ALS-associated proteins from SGs in SG-enriched fractions. Indeed, the planar compound mitoxantrone decreased association of TDP-43 Δ NLS (86–414) with SGs in H4 cells. These results perhaps reveal for the first time how putative SG shell proteins may be recruited to SG cores via RNA-dependent mechanisms, which can be disrupted by planar compounds. This observation of pre-existing structures versus proteins that assemble onto SGs later during stress motivates future systematic enumeration of core versus shell proteins, as well as functional screens to assess the differential contributions of core and shell proteins to SG formation.

SG formation has been reported to alter nucleocytoplasmic shuttling and localization of ALS-associated RBPs in a *Drosophila melanogaster* model of neurodegeneration (Zhang et al., 2018). Given this, we developed a model system of ALS/FTD and demonstrated accumulation of TDP-43 into cytoplasmic puncta during puromycin stress, which persisted into the stress recovery period in *TARDBP* and *FUS* mutant but not control iPS-MNs. This represents the first iPS-MN disease model that ties together SGs with a persistent molecular TDP-43 phenotype resembling the cytoplasmic mislocalization of TDP-43 in patient tissues. Excitingly, planar compounds produced a lasting reduction of TDP-43 accumulation into cytoplasmic puncta. This reduction is further supported by statistically significant improved survival of mouse primary neurons expressing mutant TDP-43(M337V) protein when treated with planar compounds. However, it remains to be seen whether this planar compound-mediated survival benefit corresponds with reduced mislocalization of TDP-43 into cytoplasmic foci in these neurons.

Figure 8. Planar Compounds Reduce Persistent Cytoplasmic TDP-43 Puncta in iPS-MNs

(A and B) Representative IF images (A) and quantification of cytoplasmic TDP-43 puncta area/nuclei area (B) of iPS-MNs treated with SG inhibiting compounds (5 μ M, 12 h) and stressed with puromycin (5 μ g/mL, 12 h). Arrows: cytoplasmic TDP-43 and G3BP1 puncta. Arrowheads: G3BP1-only puncta. *p < 0.05, two-sample t tests to DMSO. Bars are mean \pm SEM, n \geq 5 biological replicates of each of four control, four *TARDBP* mutant, and two *FUS* mutant lines. Scale bar is 20 μ m (5 μ m for inset).

(C and D) Representative IF images (C) and quantification of cytoplasmic TDP-43 puncta area/nuclei area (D) of iPS-MNs pre-treated with SG inhibiting compounds (2 μ M, 60 min), stressed with puromycin (5 μ g/mL, 6 h) and allowed to recover following puromycin washout (7 h). Arrows: cytoplasmic TDP-43 puncta. **p < 0.01, two-sample t tests to puromycin-stressed, DMSO-treated cells. Bars are mean \pm SEM, n = 12 biological replicates of each of four *TARDBP* mutant lines. Scale bar is 20 μ m (10 μ m for inset).

(E) Model of SG formation and progression to persistent cytoplasmic TDP-43 puncta. See discussion for full description. RBP, RNA-binding protein; IDR, intrinsically disordered region.

See also Figure S8.

These results pave the way for future testing in survival assays that integrate other genetic mutations and stressors.

Our findings that blocking SG-association of TDP-43 during transient stress prevents the subsequent formation of aggregates is seemingly in contrast to recent reports suggesting that SG localization and RNA binding can protect TDP-43 from phosphorylation and toxic phase transition (Mann et al., 2019; McGurk et al., 2018). It is very likely that the exact relationship between SG-association and insoluble aggregation of TDP-43 depends on many factors, including cell type, the specific mutations in TDP-43 and the nature and duration of the stress. In our puromycin stress paradigm in iPS-MNs, SGs form over a period of 6–24 h, which is considerably longer than the 60 min arsenite treatments used in other studies. It has been shown for TDP-43 and other ALS-associated RBPs that the initial reversible phase separation into a liquid-like state can progress toward an irreversible transition into fibrous aggregates (Patel et al., 2015). This transition is time dependent, and we therefore hypothesize that our extended SG induction is a substantially stronger driver toward permanent aggregation than those used in other studies.

Overall, our results point us toward a two-step model for SG formation (Figure 8E): In the first step (1), pre-existing G3BP1-containing subcomplexes mediate formation of a SG “core”-like assembly. In the second step (2), RBPs condense onto SGs through RNA-dependent interactions and recruit additional RNAs and IDR-containing proteins to extend the SG shell. We posit that this second step is most relevant to disease pathophysiology: mutant SG proteins accumulate in local high concentrations in SGs, which over a lifetime of stress could predispose nucleation of pathological aggregations of mutant protein, such as those seen in spinal cord MNs of ALS patients (Blokhuis et al., 2013). In this context, compounds with planar moieties could directly interact with RNAs and/or RBPs, disrupt recruitment of mutant proteins into SGs, and reduce progression to pathological protein aggregates. Thus, small-molecule disruption of RNA-RBP interactions in SGs is a potential therapeutic strategy for ALS/FTD.

STAR★METHODS

Detailed methods are provided in the online version of this paper and include the following:

- KEY RESOURCES TABLE
- LEAD CONTACT AND MATERIALS AVAILABILITY

- **EXPERIMENTAL MODEL AND SUBJECT DETAILS**
 - Generating control and mutant hiPSCs
 - Generating hiPSC-derived NPCs
 - Generating human iPS-MNs
 - G3BP1-GFP reporter and plasmid construction
 - Cell culture conditions
 - Coating plates for cell culture maintenance
 - Coating plates for primary & counterscreens
- **METHOD DETAILS**
 - Primary screen assay
 - Robotic imaging of primary screen plates
 - Automated image segmentation & quantification
 - Counterscreen assays
 - Hit compound stock solutions
 - IF and WB antibody dilutions
 - Western blot for eIF2 α .ser51 phosphorylation
 - Western blot for puromycin incorporation
 - Hit compound inhibition of SGs in iPS-MNs
 - Isolation of SG-enriched fraction
 - Western blot for RBPs in SG-enriched fraction
 - IF probing for RBPs in SG-enriched fraction
 - Silver staining of SG-enriched fraction
 - Disrupt SG-RBP association in SG fraction
 - Disrupt SG-TDP-43ΔNLS association in H4 cells
 - iPS-MN puromycin stress and recovery assays
 - iPS-MN stress and recovery with compounds
 - Neuronal survival assay with compounds
- **QUANTIFICATION AND STATISTICAL ANALYSIS**
 - Statistical analysis of screen data
 - Computing Z' for the primary screen assay
 - Estimating IC₅₀s of SG inhibiting compounds
 - Manders' co-localization measure
- **DATA AND CODE AVAILABILITY**
 - Screen hit identification pipeline
 - Screen raw data
 - Raw and analyzed data

SUPPLEMENTAL INFORMATION

Supplemental Information can be found online at <https://doi.org/10.1016/j.neuron.2019.05.048>.

ACKNOWLEDGMENTS

We thank Sheng Ding for the UCSF and Genentech Neuroprotective Libraries. We acknowledge members of the G.W.Y. lab for critical comments. M.Y.F. was supported by an NIH Ruth L. Kirschstein National Research Service Award Institutional Research Training Grant T32 DK 7541-30. S.M. was supported by a postdoctoral fellowship from the Larry L. Hillblom Foundation (2014-A-027-FEL). This work was partially supported by grants from the NIH (HG004659 to G.W.Y.), TargetALS (to G.W.Y., S.F., and J.W.L.), the ALS Association (to G.W.Y. and S.F.), and the Taube-Koret Foundation (to S.F.).

AUTHOR CONTRIBUTIONS

Conceptualization, M.Y.F., S.M., and G.W.Y.; Methodology, M.Y.F., S.M., A.Q.V., A.J., W.E.D., P.J., P.J.B., and N.A.C.; Formal Analysis, M.Y.F., S.M., A.J., W.E.D., P.J., P.J.B., N.A.C., J.W.L., and D.L.; Investigation, M.Y.F., S.M., A.Q.V., W.E.D., P.J., A.B., and M.Y.C.; Writing – Original Draft, M.Y.F.; Writing – Review & Editing, M.Y.F., S.M., W.E.D., E.L., J.W.L., and G.W.Y.; Supervision, G.W.Y.; Funding Acquisition, M.M., S.F., E.L., J.W.L., and G.W.Y.

DECLARATION OF INTERESTS

G.W.Y. is a co-founder, a member of the Board of Directors, an equity holder, on the SAB, and a paid consultant for Locana and Eclipse BiInnovations. G.W.Y. is also a visiting faculty at the National University of Singapore, Singapore. The terms of this arrangement have been reviewed and approved by the University of California, San Diego in accordance with its conflict of interest policies. The authors declare no other competing financial interests.

Received: February 26, 2019

Revised: April 28, 2019

Accepted: May 30, 2019

Published: July 1, 2019

REFERENCES

- Aittokallio, T. (2010). Dealing with missing values in large-scale studies: microarray data imputation and beyond. *Brief. Bioinform.* **11**, 253–264.
- Alami, N.H., Smith, R.B., Carrasco, M.A., Williams, L.A., Winborn, C.S., Han, S.S.W., Kiskinis, E., Winborn, B., Freibaum, B.D., Kanagaraj, A., et al. (2014). Axonal transport of TDP-43 mRNA granules is impaired by ALS-causing mutations. *Neuron* **81**, 536–543.
- Alberti, S., Halfmann, R., King, O., Kapila, A., and Lindquist, S. (2009). A systematic survey identifies prions and illuminates sequence features of prionogenic proteins. *Cell* **137**, 146–158.
- Arimoto, K., Fukuda, H., Imajoh-Ohmi, S., Saito, H., and Takekawa, M. (2008). Formation of stress granules inhibits apoptosis by suppressing stress-responsive MAPK pathways. *Nat. Cell Biol.* **10**, 1324–1332.
- Arrasate, M., Mitra, S., Schweitzer, E.S., Segal, M.R., and Finkbeiner, S. (2004). Inclusion body formation reduces levels of mutant huntingtin and the risk of neuronal death. *Nature* **431**, 805–810.
- Banani, S.F., Lee, H.O., Hyman, A.A., and Rosen, M.K. (2017). Biomolecular condensates: organizers of cellular biochemistry. *Nat. Rev. Mol. Cell Biol.* **18**, 285–298.
- Barmada, S.J., Skibinski, G., Korb, E., Rao, E.J., Wu, J.Y., and Finkbeiner, S. (2010). Cytoplasmic mislocalization of TDP-43 is toxic to neurons and enhanced by a mutation associated with familial amyotrophic lateral sclerosis. *J. Neurosci.* **30**, 639–649.
- Becker, L.A., Huang, B., Bieri, G., Ma, R., Knowles, D.A., Jafar-Nejad, P., Messing, J., Kim, H.J., Soriano, A., Auburger, G., et al. (2017). Therapeutic reduction of ataxin-2 extends lifespan and reduces pathology in TDP-43 mice. *Nature* **544**, 367–371.
- Bentmann, E., Neumann, M., Tahirovic, S., Rodde, R., Dormann, D., and Haass, C. (2012). Requirements for stress granule recruitment of fused in sarcoma (FUS) and TAR DNA-binding protein of 43 kDa (TDP-43). *J. Biol. Chem.* **287**, 23079–23094.
- Birmingham, A., Selfors, L.M., Forster, T., Wrobel, D., Kennedy, C.J., Shanks, E., Santoyo-Lopez, J., Duncan, D.J., Long, A., Kelleher, D., et al. (2009). Statistical methods for analysis of high-throughput RNA interference screens. *Nat. Methods* **6**, 569–575.
- Blokhuis, A.M., Groen, E.J., Koppers, M., van den Berg, L.H., and Pasterkamp, R.J. (2013). Protein aggregation in amyotrophic lateral sclerosis. *Acta Neuropathol.* **125**, 777–794.
- Brannan, K.W., Jin, W., Huelga, S.C., Banks, C.A., Gilmore, J.M., Florens, L., Washburn, M.P., Van Nostrand, E.L., Pratt, G.A., Schwinn, M.K., et al. (2016). SONAR Discovers RNA-Binding Proteins from Analysis of Large-Scale Protein-Protein Interactomes. *Mol. Cell* **64**, 282–293.
- Brideau, C., Gunter, B., Pikounis, B., and Liaw, A. (2003). Improved statistical methods for hit selection in high-throughput screening. *J. Biomol. Screen.* **8**, 634–647.
- Buchan, J.R., Kolaitis, R.M., Taylor, J.P., and Parker, R. (2013). Eukaryotic stress granules are cleared by autophagy and Cdc48/VCP function. *Cell* **153**, 1461–1474.

- Burkhardt, M.F., Martinez, F.J., Wright, S., Ramos, C., Volfson, D., Mason, M., Garnes, J., Dang, V., Lievers, J., Shoukat-Mumtaz, U., et al. (2013). A cellular model for sporadic ALS using patient-derived induced pluripotent stem cells. *Mol. Cell. Neurosci.* 56, 355–364.
- Carpenter, A.E., Jones, T.R., Lamprecht, M.R., Clarke, C., Kang, I.H., Friman, O., Guerini, D.A., Chang, J.H., Lindquist, R.A., Moffat, J., et al. (2006). CellProfiler: image analysis software for identifying and quantifying cell phenotypes. *Genome Biol.* 7, R100.
- Chen-Plotkin, A.S., Lee, V.M., and Trojanowski, J.Q. (2010). TAR DNA-binding protein 43 in neurodegenerative disease. *Nat. Rev. Neurol.* 6, 211–220.
- Farg, M.A., Soo, K.Y., Warraich, S.T., Sundaramoorthy, V., Blair, I.P., and Atkin, J.D. (2013). Ataxin-2 interacts with FUS and intermediate-length poly-glutamine expansions enhance FUS-related pathology in amyotrophic lateral sclerosis. *Hum. Mol. Genet.* 22, 717–728.
- Garreau de Loubresse, N., Prokhorova, I., Holtkamp, W., Rodnina, M.V., Yusupova, G., and Yusupov, M. (2014). Structural basis for the inhibition of the eukaryotic ribosome. *Nature* 513, 517–522.
- Gore, A., Li, Z., Fung, H.L., Young, J.E., Agarwal, S., Antosiewicz-Bourget, J., Canto, I., Giorgetti, A., Israel, M.A., Kiskinis, E., et al. (2011). Somatic coding mutations in human induced pluripotent stem cells. *Nature* 471, 63–67.
- Guan, L., and Disney, M.D. (2012). Recent advances in developing small molecules targeting RNA. *ACS Chem. Biol.* 7, 73–86.
- Harding, H.P., Novoa, I., Zhang, Y., Zeng, H., Wek, R., Schapira, M., and Ron, D. (2000). Regulated translation initiation controls stress-induced gene expression in mammalian cells. *Mol. Cell* 6, 1099–1108.
- Ivanov, P.A., Chudinova, E.M., and Nadezhina, E.S. (2003). Disruption of microtubules inhibits cytoplasmic ribonucleoprotein stress granule formation. *Exp. Cell Res.* 290, 227–233.
- Jain, A., and Vale, R.D. (2017). RNA phase transitions in repeat expansion disorders. *Nature* 546, 243–247.
- Jain, S., Wheeler, J.R., Walters, R.W., Agrawal, A., Barsic, A., and Parker, R. (2016). ATPase-Modulated Stress Granules Contain a Diverse Proteome and Substructure. *Cell* 164, 487–498.
- Kapeli, K., Pratt, G.A., Vu, A.Q., Hutt, K.R., Martinez, F.J., Sundaramaran, B., Batra, R., Freese, P., Lambert, N.J., Huelga, S.C., et al. (2016). Distinct and shared functions of ALS-associated proteins TDP-43, FUS and TAF15 revealed by multisystem analyses. *Nat. Commun.* 7, 12143.
- Kato, M., Han, T.W., Xie, S., Shi, K., Du, X., Wu, L.C., Mirzaei, H., Goldsmith, E.J., Longgood, J., Pei, J., et al. (2012). Cell-free formation of RNA granules: low complexity sequence domains form dynamic fibers within hydrogels. *Cell* 149, 753–767.
- Kedersha, N., and Anderson, P. (2007). Mammalian Stress Granules and Processing Bodies. *Methods Enzymol* 431, 61–81.
- Kedersha, N., Ivanov, P., and Anderson, P. (2013). Stress granules and cell signaling: more than just a passing phase? *Trends Biochem. Sci.* 38, 494–506.
- Kedersha, N., Panas, M.D., Achorn, C.A., Lyons, S., Tisdale, S., Hickman, T., Thomas, M., Lieberman, J., McInerney, G.M., Ivanov, P., and Anderson, P. (2016). G3BP-Caprin1-USP10 complexes mediate stress granule condensation and associate with 40S subunits. *J. Cell Biol.* 212, 845–860.
- Keller, B.A., Volkenning, K., Doppelmann, C.A., Ang, L.C., Rademakers, R., and Strong, M.J. (2012). Co-aggregation of RNA binding proteins in ALS spinal motor neurons: evidence of a common pathogenic mechanism. *Acta Neuropathol.* 124, 733–747.
- Khong, A., Matheny, T., Jain, S., Mitchell, S.F., Wheeler, J.R., and Parker, R. (2017). The Stress Granule Transcriptome Reveals Principles of mRNA Accumulation in Stress Granules. *Mol. Cell* 68, 808–820.
- Kim, H.J., Kim, N.C., Wang, Y.D., Scarborough, E.A., Moore, J., Diaz, Z., MacLea, K.S., Freibaum, B., Li, S., Molliex, A., et al. (2013). Mutations in prion-like domains in hnRNPA2B1 and hnRNPA1 cause multisystem proteinopathy and ALS. *Nature* 495, 467–473.
- Kim, H.J., Raphael, A.R., LaDow, E.S., McGurk, L., Weber, R.A., Trojanowski, J.Q., Lee, V.M., Finkbeiner, S., Gitler, A.D., and Bonini, N.M. (2014). Therapeutic modulation of eIF2 α phosphorylation rescues TDP-43 toxicity in amyotrophic lateral sclerosis disease models. *Nat. Genet.* 46, 152–160.
- Korth, C., May, B.C., Cohen, F.E., and Prusiner, S.B. (2001). Acridine and phenothiazine derivatives as pharmacotherapeutics for prion disease. *Proc. Natl. Acad. Sci. USA* 98, 9836–9841.
- Krach, F., Batra, R., Wheeler, E.C., Vu, A.Q., Wang, R., Hutt, K., Rabin, S.J., Baughn, M.W., Libby, R.T., Diaz-Garcia, S., et al. (2018). Transcriptome-pathology correlation identifies interplay between TDP-43 and the expression of its kinase CK1E in sporadic ALS. *Acta Neuropathol.* 136, 405–423.
- Liu-Yesucevit, L., Bilgutay, A., Zhang, Y.J., Vanderweyde, T., Citro, A., Mehta, T., Zaaru, N., McKee, A., Bowser, R., Sherman, M., et al. (2010). Tar DNA binding protein-43 (TDP-43) associates with stress granules: analysis of cultured cells and pathological brain tissue. *PLoS ONE* 5, e13250.
- Malo, N., Hanley, J.A., Cerqueiro, S., Pelletier, J., and Nadon, R. (2006). Statistical practice in high-throughput screening data analysis. *Nat. Biotechnol.* 24, 167–175.
- Manders, E.M.M.V., Verbeek, F.J., and Aten, J.A. (1993). Measurement of co-localization of objects in dual-colour confocal images. *J. Microsc.* 169, 375–382.
- Mann, J.R., Gleixner, A.M., Mauna, J.C., Gomes, E., DeChellis-Marks, M.R., Needham, P.G., Copley, K.E., Hurtle, B., Portz, B., Pyles, N.J., et al. (2019). RNA Binding Antagonizes Neurotoxic Phase Transitions of TDP-43. *Neuron* 102, 321–338.
- Markmiller, S., Soltanieh, S., Server, K.L., Mak, R., Jin, W., Fang, M.Y., Luo, E.C., Krach, F., Yang, D., Sen, A., et al. (2018). Context-Dependent and Disease-Specific Diversity in Protein Interactions within Stress Granules. *Cell* 172, 590–604.
- Martinez, F.J., Pratt, G.A., Van Nostrand, E.L., Batra, R., Huelga, S.C., Kapeli, K., Freese, P., Chun, S.J., Ling, K., Gelboin-Burkhart, C., et al. (2016). Protein-RNA Networks Regulated by Normal and ALS-Associated Mutant HNRNPA2B1 in the Nervous System. *Neuron* 92, 780–795.
- McCombe, P.A., and Henderson, R.D. (2010). Effects of gender in amyotrophic lateral sclerosis. *Gend. Med.* 7, 557–570.
- McGurk, L., Gomes, E., Guo, L., Mojsilovic-Petrovic, J., Tran, V., Kalb, R.G., Shorter, J., and Bonini, N.M. (2018). Poly(ADP-Ribose) Prevents Pathological Phase Separation of TDP-43 by Promoting Liquid Demixing and Stress Granule Localization. *Mol. Cell* 71, 703–717.
- Mosteller, F., and Tukey, J.W. (1977). Data analysis and regression: a second course in statistics (Reading, Mass.: Addison-Wesley Pub. Co.).
- Parker, S.J., Meyerowitz, J., James, J.L., Liddell, J.R., Crouch, P.J., Kanninen, K.M., and White, A.R. (2012). Endogenous TDP-43 localized to stress granules can subsequently form protein aggregates. *Neurochem. Int.* 60, 415–424.
- Patel, A., Lee, H.O., Jawerth, L., Maharana, S., Jahnel, M., Hein, M.Y., Stoynov, S., Mahamid, J., Saha, S., Franzmann, T.M., et al. (2015). A Liquid-to-Solid Phase Transition of the ALS Protein FUS Accelerated by Disease Mutation. *Cell* 162, 1066–1077.
- Patel, A., Malinovska, L., Saha, S., Wang, J., Alberti, S., Krishnan, Y., and Hyman, A.A. (2017). ATP as a biological hydrophobe. *Science* 356, 753–756.
- Prokhorova, I., Altman, R.B., Djumagulov, M., Shrestha, J.P., Urzhumtsev, A., Ferguson, A., Chang, C.T., Yusupov, M., Blanchard, S.C., and Yusupova, G. (2017). Aminoglycoside interactions and impacts on the eukaryotic ribosome. *Proc. Natl. Acad. Sci. USA* 114, E10899–E10908.
- Ran, F.A., Hsu, P.D., Wright, J., Agarwala, V., Scott, D.A., and Zhang, F. (2013). Genome engineering using the CRISPR-Cas9 system. *Nat. Protoc.* 8, 2281–2308.
- Rayman, J.B., Karl, K.A., and Kandel, E.R. (2018). TIA-1 Self-Multimerization, Phase Separation, and Recruitment into Stress Granules Are Dynamically Regulated by Zn²⁺. *Cell Rep.* 22, 59–71.
- Reinhardt, P., Glatza, M., Hemmer, K., Tsytysura, Y., Thiel, C.S., Höng, S., Moritz, S., Parga, J.A., Wagner, L., Bruder, J.M., et al. (2013). Derivation and expansion using only small molecules of human neural progenitors for neurodegenerative disease modeling. *PLoS ONE* 8, e59252.

- Ren, J., and Chaires, J.B. (1999). Sequence and structural selectivity of nucleic acid binding ligands. *Biochemistry* 38, 16067–16075.
- Ryan, V.H., Dignon, G.L., Zerze, G.H., Chabata, C.V., Silva, R., Conicella, A.E., Amaya, J., Burke, K.A., Mittal, J., and Fawzi, N.L. (2018). Mechanistic View of hnRNP A2 Low-Complexity Domain Structure, Interactions, and Phase Separation Altered by Mutation and Arginine Methylation. *Mol. Cell* 69, 465–479.
- Schindelin, J., Arganda-Carreras, I., Frise, E., Kaynig, V., Longair, M., Pietzsch, T., Preibisch, S., Rueden, C., Saalfeld, S., Schmid, B., et al. (2012). Fiji: an open-source platform for biological-image analysis. *Nat. Methods* 9, 676–682.
- Schmidt, E.K., Clavarino, G., Ceppi, M., and Pierre, P. (2009). SUnSET, a nonradioactive method to monitor protein synthesis. *Nat. Methods* 6, 275–277.
- Schneider, C.A., Rasband, W.S., and Eliceiri, K.W. (2012). NIH Image to ImageJ: 25 years of image analysis. *Nat. Methods* 9, 671–675.
- Schneider-Poetsch, T., Ju, J., Eyler, D.E., Dang, Y., Bhat, S., Merrick, W.C., Green, R., Shen, B., and Liu, J.O. (2010). Inhibition of eukaryotic translation elongation by cycloheximide and lactimidomycin. *Nat. Chem. Biol.* 6, 209–217.
- Shang, Y., and Huang, E.J. (2016). Mechanisms of FUS mutations in familial amyotrophic lateral sclerosis. *Brain Res.* 1647, 65–78.
- Shen, M., Bellaousov, S., Hiller, M., de La Grange, P., Creamer, T.P., Malina, O., Sperling, R., Mathews, D.H., Stoilov, P., and Stamm, S. (2013). Pyrinium pamoate changes alternative splicing of the serotonin receptor 2C by influencing its RNA structure. *Nucleic Acids Res.* 41, 3819–3832.
- Sidrauski, C., McGeachy, A.M., Ingolia, N.T., and Walter, P. (2015). The small molecule ISRB reverses the effects of eIF2 α phosphorylation on translation and stress granule assembly. *eLife* 4, 4.
- Sreedharan, J., Blair, I.P., Tripathi, V.B., Hu, X., Vance, C., Rogej, B., Ackerley, S., Durnall, J.C., Williams, K.L., Buratti, E., et al. (2008). TDP-43 mutations in familial and sporadic amyotrophic lateral sclerosis. *Science* 319, 1668–1672.
- Stelzer, A.C., Frank, A.T., Kratz, J.D., Swanson, M.D., Gonzalez-Hernandez, M.J., Lee, J., Andricioaei, I., Markovitz, D.M., and Al-Hashimi, H.M. (2011). Discovery of selective bioactive small molecules by targeting an RNA dynamic ensemble. *Nat. Chem. Biol.* 7, 553–559.
- Teague, S.J., Davis, A.M., Leeson, P.D., and Oprea, T. (1999). The Design of Leadlike Combinatorial Libraries. *Angew. Chem. Int. Ed. Engl.* 38, 3743–3748.
- Turakhiya, A., Meyer, S.R., Marincola, G., Bohm, S., Vanselow, J.T., Schlosser, A., Hofmann, K., and Buchberger, A. (2018). ZFAND1 Recruits p97 and the 26S Proteasome to Promote the Clearance of Arsenite-Induced Stress Granules. *Mol. Cell* 70, 906–919.
- Vance, C., Rogej, B., Hortobágyi, T., De Vos, K.J., Nishimura, A.L., Sreedharan, J., Hu, X., Smith, B., Ruddy, D., Wright, P., et al. (2009). Mutations in FUS, an RNA processing protein, cause familial amyotrophic lateral sclerosis type 6. *Science* 323, 1208–1211.
- Wang, J., Du, J., Wu, Z., and Jin, Q. (2013). Quinacrine impairs enterovirus 71 RNA replication by preventing binding of polypyrimidine-tract binding protein with internal ribosome entry sites. *PLoS ONE* 8, e52954.
- Warner, K.D., Hajdin, C.E., and Weeks, K.M. (2018). Principles for targeting RNA with drug-like small molecules. *Nat. Rev. Drug Discov.* 17, 547–558.
- Wheeler, J.R., Matheny, T., Jain, S., Abrisch, R., and Parker, R. (2016). Distinct stages in stress granule assembly and disassembly. *eLife* 5, 5.
- Wilson, W.D., Ratmeyer, L., Zhao, M., Strekowski, L., and Boykin, D. (1993). The search for structure-specific nucleic acid-interacting drugs: effects of compound structure on RNA versus DNA interaction strength. *Biochemistry* 32, 4098–4104.
- Wippich, F., Bodenmiller, B., Trajkovska, M.G., Wanka, S., Aebersold, R., and Pelkmans, L. (2013). Dual specificity kinase DYRK3 couples stress granule condensation/dissolution to mTORC1 signaling. *Cell* 152, 791–805.
- Wong, W., Bai, X.C., Brown, A., Fernandez, I.S., Hanssen, E., Condron, M., Tan, Y.H., Baum, J., and Scheres, S.H. (2014). Cryo-EM structure of the Plasmodium falciparum 80S ribosome bound to the anti-protozoan drug emetine. *eLife* 3. Published online June 9, 2014. <https://doi.org/10.7554/eLife.03080>.
- Wright, G.W., and Simon, R.M. (2003). A random variance model for detection of differential gene expression in small microarray experiments. *Bioinformatics* 19, 2448–2455.
- Yang, Y.M., Gupta, S.K., Kim, K.J., Powers, B.E., Cerqueira, A., Wainger, B.J., Ngo, H.D., Rosowski, K.A., Schein, P.A., Ackeifi, C.A., et al. (2013). A small molecule screen in stem-cell-derived motor neurons identifies a kinase inhibitor as a candidate therapeutic for ALS. *Cell Stem Cell* 12, 713–726.
- Zhang, J.H., Chung, T.D., and Oldenburg, K.R. (1999). A Simple Statistical Parameter for Use in Evaluation and Validation of High Throughput Screening Assays. *J. Biomol. Screen.* 4, 67–73.
- Zhang, K., Daigle, J.G., Cunningham, K.M., Coyne, A.N., Ruan, K., Grima, J.C., Bowen, K.E., Wadhwa, H., Yang, P., Rigo, F., et al. (2018). Stress Granule Assembly Disrupts Nucleocytoplasmic Transport. *Cell* 173, 958–971.
- Zheng, S., Chen, Y., Donahue, C.P., Wolfe, M.S., and Varani, G. (2009). Structural basis for stabilization of the tau pre-mRNA splicing regulatory element by novantrone (mitoxantrone). *Chem. Biol.* 16, 557–566.
- Zyryanova, A.F., Weis, F., Faille, A., Alard, A.A., Crespillo-Casado, A., Sekine, Y., Harding, H.P., Allen, F., Parts, L., Fromont, C., et al. (2018). Binding of ISRB reveals a regulatory site in the nucleotide exchange factor eIF2B. *Science* 359, 1533–1536.

STAR★METHODS

KEY RESOURCES TABLE

REAGENT or RESOURCE	SOURCE	IDENTIFIER
Antibodies		
Rabbit polyclonal anti-ATAXIN2	Proteintech Group	Cat#21776-1-AP; RRID:AB_10858483
Rabbit polyclonal anti-CAPRIN1	Proteintech Group	Cat#15112-1-AP; RRID:AB_2070016
Mouse monoclonal anti-CYC (clone 7H8)	Santa Cruz Biotechnology	Cat#sc-13560; RRID:AB_627383
Rabbit polyclonal anti-DDX3	Bethyl	Cat#A300-474A; RRID:AB_451009
Rabbit polyclonal anti-DDX6	Abcam	Cat#ab40684; RRID:AB_941268
Mouse monoclonal anti-EIF2S1 (clone D-3)	Santa Cruz Biotechnology	Cat#sc-133132; RRID:AB_1562699
Rabbit monoclonal anti-EIF2S1 Phospho-Ser51 (clone E90)	Abcam	Cat#ab32157; RRID:AB_732117
Rabbit polyclonal anti-EIF4G1	MBL	Cat#RN002P; RRID:AB_1570635
Rabbit polyclonal anti-FUS/TLS	Abcam	Cat#ab70381; RRID:AB_1271242
Rabbit polyclonal anti-G3BP1	MBL	Cat#RN048PW; RRID:AB_10794608
Mouse monoclonal anti-GFAP	Millipore Sigma	Cat#NE1015; RRID:AB_2043416
Mouse monoclonal anti-HB9 (clone F-5)	Santa Cruz Biotechnology	Cat#sc-515769
Mouse monoclonal anti-HNRNPA1 (clone 4B10)	Novus	Cat#NB100-672; RRID:AB_10003087
Rabbit polyclonal anti-HNRNPA2B1	GeneTex	Cat#GTX127928; RRID:AB_2616069
Mouse monoclonal anti-ISL1 (clone 1B1)	Abcam	Cat#ab86501; RRID:AB_1951289
Rabbit polyclonal anti-NANOG	Abcam	Cat#ab80892; RRID:AB_2150114
Mouse monoclonal anti-O4 (clone 81)	Millipore Sigma	Cat#MAB345; RRID:AB_11213138
Rabbit polyclonal anti-OLIG2	Millipore Sigma	Cat#AB9610; RRID:AB_570666
Rabbit polyclonal anti-PABPC1	Abcam	Cat#ab21060; RRID:AB_777008
Mouse monoclonal anti-puromycin (clone 12D10)	Millipore Sigma	Cat#MABE343; RRID:AB_2566826
Mouse monoclonal anti-SMI-31	Millipore Sigma	Cat#NE1022; RRID:AB_2043448
Mouse monoclonal anti-TARDBP (clone 2e2-d3)	Abnova	Cat#H00023435-M01; RRID:AB_1507504
Goat monoclonal anti-TIA1 (clone C-20)	Santa Cruz Biotechnology	Cat#SC-1751; RRID:AB_2201433
Chicken polyclonal anti-TUBB3	Abcam	Cat#ab107216; RRID:AB_10899689
Rabbit polyclonal anti-UBAP2L	Bethyl	Cat#A300-533A-M; RRID:AB_2779285
Rabbit monoclonal anti-USP10 (clone EPR4261)	Abcam	Cat#ab109219
Chemicals, Peptides, and Recombinant Proteins		
Sodium (meta)arsenite	Millipore Sigma	Cat#1062771000; CAS: 7784-46-5
Thapsigargin	Tocris Bioscience Bioscience	Cat#1138; CAS: 67526-95-8
Puromycin	ThermoFisher Scientific	Cat#A1113803; CAS: 58-58-2
UCSF Neuroprotective Library	Gift of Sheng Ding	N/A
Genentech Neuroprotective Library	Gift of Sheng Ding	N/A
US Drug Collection	MicroSource Discovery Systems	N/A
International Drug Collection	MicroSource Discovery Systems	N/A
Spectrum Collection	MicroSource Discovery Systems	N/A
LOPAC1280	Millipore Sigma	N/A
Prestwick Chemical Library	Prestwick	N/A
8-hydroxyquinoline	Santa Cruz Biotechnology	Cat#sc-202896; CAS: 148-24-3
Anacardic acid	Santa Cruz Biotechnology	Cat#sc-202463A; CAS: 16611-84-0
Anisomycin	Millipore Sigma	Cat#A9789; CAS: 22862-76-6
Benzethonium	Millipore Sigma	Cat#B8879; CAS: 121-54-0
Cycloheximide	Tocris Bioscience Bioscience	Cat#970; CAS: 66-81-9

(Continued on next page)

Continued

REAGENT or RESOURCE	SOURCE	IDENTIFIER
Daunorubicin	Santa Cruz Biotechnology	Cat#sc-200921; CAS: 23541-50-6
Digitoxin	Santa Cruz Biotechnology	Cat#sc-207577A; CAS: 71-63-6
Digoxin	Millipore Sigma	Cat#D6003; CAS: 20830-75-5
Doxorubicin	Fisher Scientific	Cat#ICN15910110; CAS: 23214-92-8
Gitoxigenin	Millipore Sigma	Cat#S461954; CAS: 545-26-6
GSK2606414 (PERK inhibitor)	Apexbio	Cat#A3448; CAS: 1337531-36-8
GSK2656157 (PERK inhibitor II)	Millipore Sigma	Cat#504651; CAS: 1337532-29-2
ISRib	Millipore Sigma	Cat#SML0843; CAS: 1597403-47-8
Kenpauullone	Tocris Bioscience Bioscience	Cat#1398; CAS: 142273-20-9
Mitoxantrone	Santa Cruz Biotechnology	Cat#sc-203136A; CAS: 70476-82-3
Ouabain	Millipore Sigma	Cat#O3125; CAS: 11018-89-6
Paclitaxel	Santa Cruz Biotechnology	Cat#sc-201439; CAS: 33069-62-4
Pararosanline pamoate	Millipore Sigma	Cat#P3750; CAS: 569-61-9
PD98059 (ERK inhibitor)	Santa Cruz Biotechnology	Cat#sc-3532; CAS: 167869-21-8
Penfluridol	Santa Cruz Biotechnology	Cat#sc-255410; CAS: 26864-56-2
Proscillarin A	Santa Cruz Biotechnology	Cat#sc-202775; CAS: 466-06-8
Pyrvinium pamoate	Millipore Sigma	Cat#P0027; CAS: 3546-41-6
Quinacrine	Santa Cruz Biotechnology	Cat#sc-204222; CAS: 69-05-6
ST1	Gift of Sheng Ding	N/A
Typhostin A9	Santa Cruz Biotechnology	Cat#sc-200568; CAS: 10537-47-0
WS3	Millipore Sigma	Cat#SML0758; CAS: 1421227-52-2
mTeSR1 with supplement	StemCell Technologies	Cat#85850
Dorsomorphin	Tocris Bioscience	Cat#3093; CAS: 866405-64-3
SB431542	Tocris Bioscience	Cat#1614; CAS: 301836-41-9
DMEM/F12, GlutaMAX supplement	GIBCO	Cat#10565018
N-2 Supplement	GIBCO	Cat#17502048
CTS B27 Supplement, XenoFree	GIBCO	Cat#A1486701
L-Ascorbic acid	Millipore Sigma	Cat#A4544; CAS: 50-81-7
CHIR99021	Tocris Bioscience	Cat#4423; CAS: 252917-06-9
Purmorphamine	Tocris Bioscience	Cat#4551; CAS: 483367-10-8
Y-27632	Tocris Bioscience	Cat#1254; CAS: 129830-38-2
Smoothened Agonist, SAG	Millipore Sigma	Cat#566660; CAS: 912545-86-9
Retinoic acid	Millipore Sigma	Cat#R2625; CAS: 302-79-4
DAPT	Tocris Bioscience	Cat#2634; CAS: 208255-80-5
Recombinant human BDNF	PeproTech	Cat#450-02
Recombinant human CNTF	PeproTech	Cat#450-13
Recombinant human GDNF	PeproTech	Cat#450-10
Poly-D-lysine hydrobromide	Millipore Sigma	Cat#P6407; CAS: 27964-99-4
Poly-L-ornithine hydrobromide	Millipore Sigma	Cat#P3655; CAS: 27378-49-0
Matrigel, hESC-Qualified	Corning	Cat#354277
Laminin Mouse Protein, Natural	ThermoFisher Scientific	Cat#23017015
Critical Commercial Assays		
CytoTune-iPS Sendai Reprogramming Kit	ThermoFisher Scientific	Cat#A1378001
Pierce BCA Protein Assay Kit	ThermoFisher Scientific	Cat#23225
Pierce Silver Stain Kit	ThermoFisher Scientific	Cat#24612
Deposited Data		
Screen raw data	This paper; Mendeley Data	https://doi.org/10.17632/6jpt8b7g8t.1
Raw and analyzed data	This paper; Mendeley Data	https://doi.org/10.17632/6jpt8b7g8t.1

(Continued on next page)

Continued

REAGENT or RESOURCE	SOURCE	IDENTIFIER
Experimental Models: Cell Lines		
Human: HEK293xT cells	Clontech	Cat#632180
Human: HEK293xT cells: G3BP1-GFP	This paper	N/A
Human: CV-B hiPSC	Gore et al., 2011	N/A
Human: CV-B hiPSC: G3BP1-GFP	This paper	N/A
Human: CV-B NPC: G3BP1-GFP	This paper	N/A
Human: CV-B iPS-MN: G3BP1-GFP	This paper	N/A
Human: H4	ATCC	Cat#HTB-148; RRID:CVCL_1239
Human: Kin1ALS6.2 hiPSC	This paper	N/A
Human: Kin1ALS6.3 hiPSC	This paper	N/A
Human: Kin2ALS6.4 hiPSC	This paper	N/A
Human: Kin1ALS17.3 hiPSC	Krach et al., 2018	N/A
Human: Kin3ALS6.4 hiPSC: TDP-43 N352S	This paper	N/A
Human: Kin2ALS17.5 hiPSC: TDP-43 N352S	This paper	N/A
Human: ALS17.5 hiPSC: TDP-43 N352S	Krach et al., 2018	N/A
Human: 47d hiPSC: TDP-43 G298S	Alami et al., 2014	N/A
Human: GY6.2 hiPSC: FUS R521G	Kapeli et al., 2016	N/A
Human: GY7.3 hiPSC: FUS R521G	Kapeli et al., 2016	N/A
Human: Kin1ALS6.2 iPS-MN	This paper	N/A
Human: Kin1ALS6.3 iPS-MN	This paper	N/A
Human: Kin2ALS6.4 iPS-MN	This paper	N/A
Human: Kin1ALS17.3 iPS-MN	This paper	N/A
Human: Kin3ALS6.4 iPS-MN: TDP-43 N352S	This paper	N/A
Human: Kin2ALS17.5 iPS-MN: TDP-43 N352S	This paper	N/A
Human: ALS17.5 iPS-MN: TDP-43 N352S	This paper	N/A
Human: 47d iPS-MN: TDP-43 G298S	This paper	N/A
Human: GY6.2 iPS-MN: FUS R521G	This paper	N/A
Human: GY7.3 iPS-MN: FUS R521G	This paper	N/A
Oligonucleotides		
Amplification of 5' arm of homology for G3BP1-GFP donor plasmid: G3BP_5AoH_v15_Ndel_F: TCAGAGCAGATTGTACTGAGAGTCAC CATA TG TCCCCGGCCCTTAGTTGCTAGTCCT	Markmiller et al., 2018	N/A
Amplification of 5' arm of homology for G3BP1-GFP donor plasmid: V5_loxP_1-15_R: TGCTAT ACGAAGTTATcgtagaatcgagaccgaggagggtta gggataggcttaccGA	Markmiller et al., 2018	N/A
Amplification of 3' arm of homology for G3BP1-GFP donor plasmid: G3BP_3AoH_SP_Sall_F: cggcatggacgagctgtacaagtaaGTCGACATCTTCA TGGATCTCATGCAGCCATACA	Markmiller et al., 2018	N/A
Amplification of 3' arm of homology for G3BP1-GFP donor plasmid: G3BP_3AoH_v12_HR_SphI_R: AGCTATGACCATGATTACGCCAAGCTT GCATGC CCATCAATAAAAGAGAACCATACA	Markmiller et al., 2018	N/A
Cloning of G3BP1 gRNAs into px458 Cas9 expression plasmid: G3BP1_gRNA4_F: caccTCATGCAGCCATACAAACCC	Markmiller et al., 2018	N/A
Cloning of G3BP1 gRNAs into px458 Cas9 expression plasmid: G3BP1_gRNA4_R: aaacGGTTTGATGGCTGCATGA	Markmiller et al., 2018	N/A

(Continued on next page)

Continued

REAGENT or RESOURCE	SOURCE	IDENTIFIER
Cloning of G3BP1 gRNAs into px458 Cas9 expression plasmid: G3BP1_gRNA5_F: caccTCCATGAAGATTCACTGCCG	Markmiller et al., 2018	N/A
Cloning of G3BP1 gRNAs into px458 Cas9 expression plasmid: G3BP1_gRNA5_R: aaacCGGCAGTGAAATCTTCATGGAA	Markmiller et al., 2018	N/A
Integration mapping of GFP into <i>G3BP1</i> locus: G3BP_intmap_F1: AGCCACTGAAGAACCCAGAA	Markmiller et al., 2018	N/A
Recombinant DNA		
HR120PA-1 targeting vector	System Biosciences	Cat#HR120PA-1
pSpCas9(BB)-2A-GFP (PX458)	Gift from Feng Zhang; Ran et al., 2013	Addgene plasmid #48138; RRID:Addgene_48138
pLVX-CMV_IRES-Hygro	Clontech	Cat#632182
pLVX-TetOne_IRES-Puro	Clontech	Cat#631847
Software and Algorithms		
Image segmentation with CellProfiler	Carpenter et al., 2006	https://www.cellprofiler.org/
SWIMMER pipeline for identifying hits with random variance modeling	This paper	https://github.com/YeoLab
Image colocalization with ImageJ	Schindelin et al., 2012	https://imagej.net/Coloc_2

LEAD CONTACT AND MATERIALS AVAILABILITY

Further information and requests for resources and reagents should be directed to and will be fulfilled by the Lead Contact, Gene W. Yeo (gene.yeo@ucsd.edu).

EXPERIMENTAL MODEL AND SUBJECT DETAILS

Generating control and mutant hiPSCs

CV-B human induced pluripotent stem cells were obtained courtesy of Lawrence S.B. Goldstein, as described (Gore et al., 2011). Human induced pluripotent stem cell (hiPSC) lines carrying ALS-associated mutations in *TARDBP* (N352S) and control individuals were previously reprogrammed from primary fibroblasts obtained by Dr. John Ravits (University of California, San Diego), as described (Krach et al., 2018). Lines carrying *TARDBP* (G298S) mutations were obtained courtesy of Kevin Eggan, as described (Alami et al., 2014). Lines carrying ALS-associated *FUS* (R521G) mutations were previously reprogrammed from primary fibroblasts obtained by Franca Cambi, Edward Kasarskis and Haining Zhu (University of Kentucky), as described (Kapeli et al., 2016). Reprogramming of all fibroblasts was performed with the CytoTune-iPS Sendai Reprogramming Kit. In total, hiPSC lines were generated from three control individuals, four individuals with mutations in *TARDBP* and two individuals with mutations in *FUS*. Four hiPSC lines from the three control individuals, four hiPSC lines from the four individuals with mutations in *TARDBP* and two hiPSC lines from the two individuals with mutations in *FUS* were concurrently differentiated into four control, four *TARDBP* mutant and two *FUS* mutant iPS-MN lines, respectively. The sex of these hiPSC lines differentiated into iPS-MNs are as follows. Four control hiPSC lines: Kin1ALS6.2 (female), Kin1ALS6.3 (female), Kin2ALS6.4 (male), Kin1ALS17.3 (female). Four *TARDBP* mutant hiPSC lines: Kin3ALS6.4 (female), Kin2ALS17.5 (male), ALS17.5 (male), 47d (male). Two *FUS* mutant hiPSC lines: GY6.2 (male), GY7.3 (male). For completeness, the sex of HEK293xT cells is female, CV-B hiPSC is male and H4 cells is male (Gore et al., 2011). Informed consent was obtained from all individuals prior to biopsy and the use of human fibroblasts for this project was approved by the University of California, San Diego Institutional Review Board.

Generating hiPSC-derived NPCs

Generation of small molecule neural precursor cells (NPCs) from hiPSCs was adapted from a previously reported protocol (Reinhardt et al., 2013). Briefly, hiPSCs were dissociated into single cells with Accutase and 3×10^6 cells were seeded into one well of an uncoated 6-well plate. The plate was incubated on an orbital shaker at 90 rpm at 37°C, 5% CO₂ and the cells were grown in DMEM/F12, GlutaMAX supplement media containing N-2 Supplement (1:100 v/v), CTS B27 Supplement, XenoFree (1:50 v/v), L-ascorbic acid (150 μM), CHIR99021 (3 μM), purmorphamine (0.5 μM), Y-27632 (5 μM), as well as two small molecule SMAD inhibitors: SB431542 (10 μM) and dorsomorphin (1 μM). After 2 days, embryoid bodies (EB) formed, at which point 1/3 of the EBs were transferred to three wells of an uncoated 6-well plate to prevent overgrowth; Y-27632 was also withdrawn from the media. Following

this passaging, half media changes were performed every 24 hours. At 6 days, formation of neuroepithelium was evident in the EBs and a full media change was performed to media that omits SB431542 and dorsomorphin (NPC media, also described below). At 8 days, individual EBs were picked and triturated into small fragments. These EB fragments were seeded onto 10 cm plates coated with Matrigel. These plates were prepared by adding 6 mL of Matrigel (diluted 1:60 v/v in DMEM/F12, GlutaMAX supplement) to each 10 cm plate and incubating for 60 min. EB fragments were maintained on these Matrigel plates as adherent cultures. After 4 days, these adherent EB fragments were dissociated into single cells with Accutase and passaged at a ratio of 1:6 to 1:8 onto new Matrigel plates. Every 3–6 days thereafter these cultures were passaged at a 1:10 to 1:15 ratio. After 5–6 passages, most non-NPCs disappear and homogeneous colonies of NPCs remained. These NPCs may be passaged at least 20 times at a 1:5 to 1:15 ratio.

Generating human iPS-MNs

Generation of iPS-MNs was adapted from a previous reported protocol (Martinez et al., 2016). All hiPSC lines were concurrently differentiated into iPS-MNs. Briefly, hiPSCs were dissociated into single cells with Accutase and 1×10^6 cells were seeded into one well of a Matrigel-coated 6-well plate. These Matrigel-coated plates were prepared by adding 1 mL of Matrigel (diluted 1:60 v/v in DMEM/F12, GlutaMAX supplement) to each well of a 6-well plate and incubating the plate for 60 min. The dissociated hiPSCs were grown for 6 days in DMEM/F12, GlutaMAX supplement media containing N-2 Supplement (1:100 v/v), CTS B27 Supplement, XenoFree (1:50 v/v), L-ascorbic acid (150 μ M), CHIR99021 (3 μ M), as well as two small molecule SMAD inhibitors: SB431542 (10 μ M) and dorsomorphin (1 μ M). ROCK inhibitor (Y-27632) may also be added to the media to a final concentration of 5 μ M to reduce cell death. Full media changes were performed every 24 hours. At 7 days, a full media change was performed in which CHIR99021 was withdrawn from the media and retinoic acid (1.5 μ M) and Smoothened Agonist (200 nM) was added to the media. The cells were cultured for a further 8 days in this media with daily full media changes. At 15 days, the cells were dissociated: Cells were washed once with PBS and 3 mL of Accutase was added per well of a 6-well plate. Cells were incubated with Accutase for 30 min. Next, each well of cells was triturated gently 4–5 times, transferred to 15 mL centrifuge tubes containing 6 mL of DMEM/F12, GlutaMAX supplement and the cells pelleted by centrifuging for 5 min at 1000 g. The cell pellets should be resuspended and 1×10^7 cells seeded onto each 10 cm Matrigel-coated plate; the media should also be supplemented with 10 μ M Y-27632 to reduce cell death. Full media changes were performed every 24 hours. At 20 days, the media was modified to reduce Y-27632 (2 μ M) and to include three growth factors: recombinant human BDNF (2 ng/mL), recombinant humanCNTF (2 ng/mL) and recombinant human GDNF (2 ng/mL). At 22 days, retinoic acid and Smoothened Agonist were withdrawn from the media and DAPT (2 μ M) was added to aid maturation to iPS-MNs. At this point, full media changes were performed every 2 days. At 26 days, DAPT was withdrawn from the media. At 28 days, iPS-MN cultures were obtained that stained positive for known MN markers Hb9, Islet-1/2 and SMI-31.

G3BP1-GFP reporter and plasmid construction

To generate G3BP1-GFP HEK293xT and CV-B hiPSC SG reporter lines, the HR120PA-1 targeting vector (System Biosciences) was modified to include a 1.5 kilobase 5' arm of homology spanning part of intron 11 and exon 12 of the endogenous human G3BP1 locus and a 1.5 kilobase 3' arm of homology from the 3' untranslated region of G3BP1. These arms of homology were amplified from genomic DNA using the primers G3BP_5AoH_v15_Ndel_F and V5_loxP_1-15_R for the 5' arm of homology and G3BP_3AoH_SP_Sall_F and G3BP_3AoH_v12_HR_SphI_R for the 3' arm of homology. The modified G3BP1 targeting vector was assembled via Gibson assembly. To generate Cas9 expression vectors targeting the endogenous G3BP1 locus, the oligo pairs G3BP1_gRNA4_F, G3BP1_gRNA4_RCas9 and G3BP1_gRNA5_F, G3BP1_gRNA5_R were inserted into the Cas9 expression vector pSpCas9(BB)-2A-GFP (PX458) (Ran et al., 2013). HEK293xT cells were transfected with the targeting vector and the two Cas9 expression vectors using lipofectamine 2000. CV-B hiPSCs were electroporated using an Amaxa Nucleofector with Stem Cell Kit 1 and pulse setting B-016. Cells were selected beginning two days after transfection with puromycin at 1 μ g/mL for four days. After two weeks, G3BP1-GFP colonies were picked using a steromicroscope. Correct insertion was validated with the sequencing primer G3BP_intmap_F1. G3BP1-GFP CV-B hiPSCs were subsequently differentiated to NPCs and iPS-MNs as described above.

Cell culture conditions

Human induced pluripotent stem cells (hiPSCs) were maintained in mTeSR1 with supplement. hiPSCs were clump dissociated and passaged using enzyme-free Cell Dissociation Buffer. HEK293xT cells were maintained in DMEM, high glucose supplemented with 10% fetal bovine serum, heat inactivated. HEK293xT cells were dissociated and passaged using TrypLE Express Enzyme dissociation buffer. Small molecule neural precursor cells (NPCs) were maintained in DMEM/F12, GlutaMAX supplement, containing N-2 Supplement (1:100 v/v), CTS B27 Supplement, XenoFree (1:50 v/v), L-ascorbic acid (150 μ M), CHIR99021 (3 μ M) and purmorphamine (0.5 μ M). NPCs were dissociated and passaged using Accutase solution. iPS-MNs were maintained in DMEM/F12, GlutaMAX supplement, containing N-2 Supplement (1:100 v/v), CTS B27 Supplement, XenoFree (1:50 v/v), L-ascorbic acid (150 μ M), recombinant human BDNF (2 ng/mL), recombinant human CNTF (2 ng/mL) and recombinant human GDNF (2 ng/mL). iPS-MNs were dissociated and passaged using Accumax solution. All cell types were cultured in humidified incubators at 37°C, 5% CO₂.

Coating plates for cell culture maintenance

For HEK293xT cells, 10 cm tissue culture plates were coated with 4 mL aqueous solution of 0.001% w/v poly-D-lysine (PDL) hydrobromide and incubated for 5 min. The PDL was then aspirated and the plates washed once with sterile water. For human induced pluripotent stem cells and small molecule neural precursor cells (NPCs), 10 cm tissue culture plates were coated with 6 mL of Matrigel (diluted 1:60 v/v in DMEM/F12, GlutaMAX supplement) and incubated for 60 min. The Matrigel was then aspirated and the plates seeded with cells. For iPS-MNs, 10 cm tissue culture plates were coated with 4 mL aqueous solution containing 0.001% w/v PDL hydrobromide and 0.001% w/v poly-L-ornithine (PLO) hydrobromide and incubated overnight. The PDL/PLO was then aspirated and the plates washed once with sterile water. Next the plates were coated with 6 mL of mouse laminin (20 µg/mL in NPC media without CHIR99021 and purmorphamine) and incubated overnight. Finally, the laminin was aspirated and the plates were seeded with cells.

Coating plates for primary & counterscreens

For HEK293xT cells, 384-well plates were coated by adding 10 µL of 0.001% w/v poly-D-lysine (PDL) hydrobromide to each well and incubating overnight. The PDL was then aspirated and the wells washed once with sterile water. For small molecule neural precursor cells (NPCs), 384-well plates were coated by adding 10 µL of 0.001% w/v PDL to each well and incubating overnight. The PDL was then aspirated and the wells washed once with sterile water. Next, 15 µL of mouse laminin (20 µg/mL in NPC media without CHIR99021 and purmorphamine) was added to each well and incubated overnight. Finally, the laminin was aspirated and the plates were seeded with cells. For iPS-MNs, 384-well plates were coated by adding 10 µL of 0.001% w/v PDL + 0.001% w/v poly-L-ornithine (PLO) hydrobromide to each well and incubating overnight. The PDL/PLO was then aspirated and the wells washed once with sterile water. Next, 15 µL of mouse laminin (20 µg/mL in NPC media without CHIR99021 and purmorphamine) was added to each well and incubated overnight. Finally, the laminin was aspirated and the plates were seeded with cells. Liquid handling was performed with a Hamilton Microlab STAR fluid handler.

METHOD DETAILS

Primary screen assay

Using a Hamilton Microlab STAR liquid handler, HEK293xT cells were plated at 7500 cells per well of 384-well plates in 20 µL of HEK293xT media, while the CV-B small molecule neural precursor cells (NPCs) were plated at 12000 cells per well of 384-well plates in 20 µL of NPC media without CHIR99021 or purmorphamine. Both cell types were then incubated overnight. After overnight incubation, cells were then pre-treated with screen compounds from the following compound libraries: The UCSF Neuroprotective Library and Genentech Neuroprotective Library were gifts of Sheng Ding. The US Drug Collection, International Drug Collection, Spectrum Collection, LOPAC1280 and Prestwick Chemical Library were sourced from the Conrad Prebys Center for Chemical Genomics at the Sanford Burnham Prebys Medical Discovery Institute, La Jolla Campus. Using a Labcyte ECHO 555 Liquid Handler, compounds from these libraries were spotted into the wells of two to four biological duplicates at a final concentration of 10 µM and cells were incubated with compounds for 60 min. After compound pre-treatment, cells were stressed by using the Hamilton fluid handler to add NaAsO₂ diluted in 20 µL of DMEM to each well, to a final concentration of 500 µM or 250 µM of NaAsO₂ for HEK293xT cells or NPCs, respectively. Cells were incubated with NaAsO₂ for 60 min. Finally, cells were fixed by adding 24% paraformaldehyde in PBS to each well to a final concentration of 4% and incubated for 45 min at room temperature. After fixing, the plates were washed three times with PBS. Nuclei were stained with 30 µL DAPI (1:5000 v/v in PBS) per well and incubated overnight at 4°C, after which the plates were washed once with PBS. Finally, to preserve the plates 30 µL of 50% v/v glycerol in PBS was added to each well. Cells were imaged in this glycerol solution.

Robotic imaging of primary screen plates

Screen plates were imaged using a Thermo Scientific CRS CataLyst-5 Express robotic plate loader coupled with a GE Healthcare IN Cell Analyzer 1000 plate imager. Four fields at the center of each well were imaged with a 10 × objective through 460 nm and 535 nm emission filters for DAPI and G3BP1-GFP, respectively. Images at 460 nm and 535 nm were taken with 250 ms and 750 ms exposures, respectively.

Automated image segmentation & quantification

SG screen and secondary assay images were segmented and image features quantified using a custom CellProfiler pipeline (Carpenter et al., 2006). Briefly, nuclei were segmented and identified in the DAPI fluorescence channel images using a diameter cutoff of 9–80 pixels for HEK293xT cells, small molecule neural precursor cells (NPCs) and iPS-MNs. Cell bodies were then extrapolated by overlaying the GFP fluorescence channel images and tracing radially outward from the nuclei to the limits of the cytoplasmic G3BP1-GFP signal. The cell bodies were used as masks to eliminate imaging artifacts outside of cell boundaries, such as background fluorescence or dead cells. After masking, punctate structures were enhanced by image processing for speckle-like features that were 10 pixels in diameter for HEK293xT cells or 7 pixels in diameter for NPCs and iPS-MNs and these punctate structures were then annotated as features such as G3BP1-GFP SGs or TDP-43 puncta. Finally, the total image area which was enclosed in each of the identified features (nuclei, punctate structures or intersections of features) was calculated and output to spreadsheets.

Counterscreen assays

384-well plates were coated as described above for 384-well primary and counterscreen plates and HEK293xT cells or NPCs were seeded as described above for the primary screen assay. For dose response assays, hit compounds diluted in 20 µL DMEM were added to cells to final concentrations of 30, 10, 3.3, 1.1, 0.37 or 0.12 µM and cells were incubated with compounds for 60 min. Cells were then stressed by adding NaAsO₂ diluted in 40 µL of DMEM to each well, to a final concentration of 500 µM or 250 µM for HEK293xT cells or CV-B small molecule neural precursor cells (NPCs), respectively. Cells were incubated with NaAsO₂ for 60 min at 37°C, 5% CO₂, after which cells were fixed, DAPI stained and imaged. For heat shock stress assays, hit compounds diluted in 20 µL DMEM were added to cells to final concentrations of 10 µM and cells were incubated with compounds for 60 min. Cells were then heat shocked by incubating for 60 min at 43°C, 5% CO₂, after which cells were fixed, DAPI stained and imaged. For thapsigargin stress assays, hit compounds diluted in 20 µL DMEM were added to cells to final concentrations of 10 µM and cells were incubated with compounds for 60 min. Cells were then stressed by adding thapsigargin diluted in 40 µL DMEM to a final concentration of 50 µM or 1 µM for HEK293xT cells or NPCs, respectively. Cells were then incubated with thapsigargin for 60 min at 37°C, 5% CO₂, after which cells were fixed, DAPI stained and imaged. For the NaAsO₂ pre-stress assays, cells were first stressed by adding NaAsO₂ diluted in 20 µL DMEM to a final concentration of 250 µM or 100 µM for HEK293xT cells or NPCs, respectively. Cells were incubated with NaAsO₂ for 60 min. Then, hit compounds diluted in 40 µL DMEM were added to cells to a final concentration of 10 µM and cells were incubated with compounds for 60 min at 37°C, 5% CO₂, after which cells were fixed, DAPI stained and imaged. For the assays in which unstressed cells were incubated with hit compounds, compounds diluted in 20 µL DMEM were added to cells to final concentrations of 10 µM and cells were incubated with compounds for 60 min at 37°C, 5% CO₂, 40 µL DMEM without NaAsO₂ was added to each well and cells were further incubated for 60 min at 37°C, 5% CO₂, after which cells were fixed, DAPI stained and imaged. For the assays in S2 cells, compounds were added to cells to final concentrations of 30 µM for 60 min. NaAsO₂ was added to cells to a final concentration of 500 µM for a further 60 min, after which cells were fixed, stained for Rasputin, DAPI stained and imaged.

Hit compound stock solutions

The following hit compounds were solubilized in DMSO to 10 mM stock solutions for counterscreens and secondary assays: 8-hydroxyquinoline, anacardic acid, anisomycin, benzethonium, cycloheximide, daunorubicin, digitoxin, digoxin, doxorubicin, gitoxigenin, GSK2606414 (PERK inhibitor), GSK2656157 (PERK inhibitor II), ISRIB, kenpaullone, mitoxantrone, ouabain, paclitaxel, pararosanline pamoate, PD98059 (ERK inhibitor), penfluridol, proscillarin A, pyrinium pamoate, quinacrine, ST1, tyrphostin A9 and WS3.

IF and WB antibody dilutions

Antibodies were used at the following dilutions: rabbit polyclonal anti-ATAXIN2 (IF: 1:100, WB: 1:500), rabbit polyclonal anti-CAPRIN1 (IF: 1:100, WB: 1:1000), mouse monoclonal anti-CYC (clone 7H8) (IF: 1:500), rabbit polyclonal anti-DDX3 (IF: 1:1000, WB: 1:1000), rabbit polyclonal anti-DDX6 (IF: 1:1000), mouse monoclonal anti-EIF2S1 (clone D-3) (WB: 1:1000), rabbit monoclonal anti-EIF2S1 Phospho-Ser51 (clone E90) (WB: 1:1000), rabbit polyclonal anti-EIF4G1 (IF: 1:500), rabbit polyclonal anti-FUS/TLS (IF: 1:1000, WB: 1:1000), rabbit polyclonal anti-G3BP1 (IF: 1:500, WB: 1:2000), mouse monoclonal anti-GFAP (IF: 1:500), mouse monoclonal anti-HB9 (clone F-5) (IF: 1:100), mouse monoclonal anti-HNRNPA1 (clone 4B10) (IF: 1:200), rabbit polyclonal anti-HNRNPA2B1 (IF: 1:500, WB: 1:1000), mouse monoclonal anti-ISL1 (clone 1B1) (IF: 1:1000), rabbit polyclonal anti-NANOG (IF: 1:500), mouse monoclonal anti-O4 (clone 81) (IF: 1:100), rabbit polyclonal anti-OLIG2 (IF: 1:500), rabbit polyclonal anti-PABPC1 (IF: 1:500, WB: 1:1000), mouse monoclonal anti-puromycin (WB: 1:1000), mouse monoclonal anti-SMI-31 (IF: 1:1000), mouse monoclonal anti-TARDBP (clone 2e2-d3) (IF: 1:100, WB: 1:1000), goat monoclonal anti-TIA1 (clone C-20) (IF: 1:250, WB: 1:500), chicken polyclonal anti-TUBB3 (IF: 1:1000), rabbit polyclonal anti-UBAP2L (IF: 1:500, WB: 1:1000) and rabbit monoclonal anti-USP10 (clone EPR4261) (IF: 1:500, WB: 1:1000).

Western blot for eIF2α ser51 phosphorylation

12-well plates were coated as described above for 384-well primary and counterscreen plates but scaled to 12-well plates. 2*10⁵ HEK293xT cells or CV-B small molecule neural precursor cells (NPCs) were seeded into each well and incubated overnight. Hit compounds diluted in DMEM were added to cells to final concentrations of 10 µM and incubated with cells for 60 min. HEK293xT cells or NPCs were then stressed by adding NaAsO₂ diluted in DMEM to final concentrations of 500 µM or 250 µM and incubated for 40 min or 60 min, respectively. Next, the media was aspirated and cells were washed once with PBS at room temperature. Cells were lysed for 10 min on ice with 100 µL per well of ice-cold RIPA Buffer Solution (Teknova) supplemented with cComplete, EDTA-free Protease Inhibitor Cocktail (1 tab/50 mL), PhosSTOP phosphatase inhibitor cocktail (1 tab/10 mL) and Benzonase nuclease cocktail (1:1000). A Pierce BCA Protein Assay Kit was used to quantify protein concentrations in lysates and 1 µg of total protein from each lysate was loaded for gel electrophoresis and western blotting. Western blot membranes were blocked with 1% bovine serum albumin (BSA) in TBST for 60 min at room temperature, probed for serine 51 phosphorylated eIF2α using rabbit anti-EIF2S1 (Phospho-Ser51) primary antibody diluted 1:1000 in 0.5% BSA in TBST overnight at 4°C and probed with secondary antibody diluted 1:2000 in 0.5% BSA in TBST for 60 min at room temperature. As control, total eIF2α was probed using rabbit anti-EIF2S1 primary

antibody. Western blot band sizes were quantified by densitometry in ImageJ: Equally sized boxes were drawn around bands and pixel intensities were integrated over the box areas to give the band sizes ([Schneider et al., 2012](#)).

Western blot for puromycin incorporation

12-well plates were coated as described above for 384-well primary and counterscreen plates but scaled to 12-well plates. 2×10^5 HEK293xT cells (not CRISPR-tagged with the G3BP1-GFP vector described above) were seeded into each well and incubated overnight. Hit compounds diluted in DMEM were added to cells to final concentrations of 10 μM and incubated with cells for 60 min. HEK293xT cells were then stressed by adding NaAsO₂ diluted in DMEM to a final concentration of 500 μM and incubated for 40 min. Next, the media was aspirated and cells were washed once with PBS at room temperature. Using puromycin incorporation into peptides as a measure of translation, cells were pulsed with 10 $\mu\text{g}/\text{mL}$ puromycin diluted in PBS for 10 min at 37°C, followed by aspiration and a 30 min chase at 37°C in HEK293xT media ([Schmidt et al., 2009](#)). After this, the media was aspirated, cells washed once with PBS at room temperature and lysed as above for WB of eIF2 α ser51 phosphorylation. A Pierce BCA Protein Assay Kit was used to verify that similar total amounts of protein in lysates were loaded for gel electrophoresis and western blotting. Western blot membranes were blocked with 5% milk in TBST for 60 min at room temperature, probed for puromycin using mouse anti-puromycin primary antibody diluted 1:1000 in 0.5% milk in TBST overnight at 4°C and probed with secondary antibody diluted 1:1000 in 0.5% milk in TBST for 60 min at room temperature. For each lysate sample, the entire lane was quantified by densitometry in ImageJ: Equally sized boxes were drawn around entire lanes for all lysate samples and pixel intensities were integrated over the box areas to give the lane quantifications ([Schneider et al., 2012](#)).

Hit compound inhibition of SGs in iPS-MNs

iPS-MNs were differentiated as described above and seeded into pre-coated 384-well plates. In brief, day 28 iPS-MNs were dissociated into single cells by adding 3 mL Accumax into each well of a 6-well plate of iPS-MNs and incubating for 60 min. The iPS-MNs were then gently triturated 10-15 times with a P1000 pipette and then incubated for a further 15 min at 37°C, 5% CO₂ to complete the dissociation. The iPS-MNs were transferred to 15 mL centrifuge tubes containing 6 mL DMEM/F12, GlutaMAX supplement and cells were pelleted by centrifuging for 4 min at 200 $\times g$. The cell pellet was then resuspended in 1 mL iPS-MN media supplemented with 10 μM Y-27632 (media formulation described above) by gently triturating 10-20 times with a P1000 pipette and cell clumps were filtered out using a 40 μm filter. 10⁴ iPS-MNs were seeded into each well of a laminin-coated 384-well plate in 20 μL of iPS-MN media; plate coating was as described above for 384-well primary and counterscreen plates. Cells were allowed to adhere by incubating for 48 hours at 37°C, 5% CO₂; iPS-MNs were fed 24 hours after seeding by adding 20 μL of iPS-MN media to each well to a final volume of 40 μL per well. For NaAsO₂ stress assays, hit compounds diluted in 20 μL media were added to iPS-MNs to a final concentration of 10 μM and cells were incubated with compounds for 80 min. iPS-MNs were then stressed by adding NaAsO₂ diluted in 20 μL iPS-MN media to a final concentration of 100 μM and incubated for 120 min at 37°C, 5% CO₂, after which cells were fixed. For thapsigargin stress assays, hit compounds diluted in 20 μL iPS-MN media were added to iPS-MNs to final concentrations of 10 μM and cells were incubated with compounds for 80 min. iPS-MNs were then stressed by adding thapsigargin diluted in 20 μL iPS-MN media to a final concentration of 250 nM and incubated for 120 min at 37°C, 5% CO₂, after which cells were fixed. For puromycin stress assays, hit compounds and puromycin were diluted in 40 μL iPS-MN media and added to iPS-MNs to final compound concentrations of 5 μM and final puromycin concentration of 5 $\mu\text{g}/\text{mL}$. iPS-MNs were incubated with compounds and puromycin for 12 hours at 37°C, 5% CO₂, after which cells were fixed. G3BP1 and TDP-43 were stained by IF according to the procedure described below for IF staining of SG-enriched fractions; nuclei were stained with DAPI. iPS-MNs were imaged as described above for robotic imaging of primary screen plates.

Isolation of SG-enriched fraction

SG-enriched fractions were isolated as described previously ([Jain et al., 2016](#)). Briefly, cells were grown in 10 cm plates to 75%-90% confluence and stressed with NaAsO₂ as described above for the primary screen assay. The media was then aspirated, cells were washed once with PBS at room temperature and then lysed for 10 minutes on ice with 6 mL ice-cold NP-40 lysis buffer per 10 cm plate; formulation of this lysis buffer is as previously described ([Jain et al., 2016](#)). Lysed cells were scraped and collected in 15 mL centrifuge tubes in 3 mL aliquots. Lysates were sonicated using a Diagenode Bioruptor Plus for two cycles of 10 s on low power and one cycle of 10 s on high power. After each sonication cycle, lysates were chilled on ice for 20 s. Following sonication, the lysates were centrifuged at 1000 g for 5 min at 4°C to pellet nuclei. The supernatants were then collected into 1.5 mL centrifuge tubes and centrifuged at 18000 g for 20 min at 4°C to pellet SGs. The pellets were resuspended by trituration in 1/10 of the original volume of ice-cold NP-40 lysis buffer. The resuspended samples were finally centrifuged at 850 g for 2 min at 4°C to pellet membrane-bound organelles and other large debris. The remaining supernatants were collected as the SG-enriched fractions. The same fractionation procedure was performed on unstressed cells as a control.

Western blot for RBPs in SG-enriched fraction

A Pierce BCA Protein Assay Kit was used to quantify protein concentrations in SG-enriched fractions and 1 μg of total protein from each sample was loaded for gel electrophoresis and western blotting. For input controls, 1 μg of total protein from whole cell lysates was also loaded. After transfer and blotting, western blot band sizes were quantified by densitometry in ImageJ as described above

for western blotting of eIF2 α ser51 phosphorylation. SG-enriched fraction band sizes were normalized by dividing by the band sizes of the corresponding input controls.

IF probing for RBPs in SG-enriched fraction

In each well of a 96-well plate, 2 μ g of total protein from SG-enriched fractions was added to 40 μ L of ice-cold NP-40 lysis buffer and SGs in these fractions were allowed to settle by incubating overnight at 4°C. To fix the SGs, 8% paraformaldehyde (PFA) in PBS was added to each well to a final concentration of 4% PFA and plates were incubated for 10 min at room temperature. The PFA was aspirated and the wells were washed three times with PBS at room temperature. Next the wells were simultaneously permeabilized and blocked by adding 80 μ L of 0.1% v/v Triton X-100 + 5% v/v serum (of the same species as secondary antibody) in PBS to each well and incubating the plates for 45 min at room temperature. The plates were then washed once with wash buffer (0.01% v/v Triton X-100 in PBS) before probing with primary antibody. Primary antibody was diluted in wash buffer containing 1% w/v bovine serum albumin (BSA). 40 μ L of primary antibody solution was added per well and plates were overnight at 4°C. Plates were then washed five times with wash buffer. Secondary antibody was diluted in wash buffer containing 1% w/v BSA. 40 μ L of secondary antibody solution was added per well and plates were incubated overnight at 4°C. Plates were washed 10 times with wash buffer, stained with DAPI overnight, washed once with wash buffer and preserved by adding 80 μ L of 50% v/v glycerol in PBS per well. Plates were then imaged at 20 \times magnification on a ZEISS Axio Vert.A1 inverted microscope or at 40 \times magnification on an Opera Phenix high content imaging system (Perkin Elmer).

Silver staining of SG-enriched fraction

A Pierce Silver Stain Kit was used to visualize relative protein abundances in total lysate inputs and SG-enriched fractions from stressed and unstressed cells. 4 μ g of total protein from each sample was loaded for gel electrophoresis. After gel electrophoresis, protein bands in the gel were stained following manufacturer's instructions.

Disrupt SG-RBP association in SG fraction

For digestion of SG-enriched fractions with RNase I, 10 μ g of total protein from SG-enriched fractions was incubated with 0, 2, 8 or 32 Units of RNase I in 1.5 mL centrifuge tubes and shaken at 1200 rpm for 5 min at 37°C using an Eppendorf Thermomixer R. The SG-enriched fractions were immediately centrifuged at 18000 \times g for 20 min at 4°C to pellet remaining SG-like structures. The pellets were resuspended in equal volume lysis buffer and analyzed by western blotting and IF staining as described above for SG-enriched fractions. For incubation with compounds, 10 μ g of total protein from SG-enriched fractions was incubated with hit compound to a final concentration of 100 μ M and nutated overnight at 4°C using a Fisherbrand Mini-Tube Rotator. After overnight incubations, the samples were plated, fixed and analyzed by IF staining as described above for SG-enriched fractions, or centrifuged at 18000 \times g for 20 min at 4°C to pellet remaining SG-like structures. The pellets were resuspended in equal volume lysis buffer and analyzed by western blotting as described above for SG-enriched fractions.

Disrupt SG-TDP-43 Δ NLS association in H4 cells

H4 cells were stably transduced with lentivirus encoding G3BP1-mCherry and doxycycline-inducible GFP-TDP-43 Δ NLS (86-414) made from pLVX-CMV_IRES-Hygro (Clontech) and pLVX-TetOne_IRES-Puro (Clontech), respectively. Cells were maintained in DMEM, high glucose supplemented with 10% fetal bovine serum, heat inactivated and grown on 10 cm PDL coated plates, prepared as described above for HEK293xT cells. H4 cells were dissociated and passaged using TrypLE Express Enzyme dissociation buffer. 2 \times 10 5 cells in 50 μ L media were seeded into each well of a 96-well plate (Perkin-Elmer). Following overnight incubation in a humidified incubator at 37°C, 5% CO₂, the cells were induced with doxycycline (1 ng/mL) for 24 hours. After doxycycline induction, hit compounds diluted in 50 μ L media were added to final concentrations of 5 μ M and cells were incubated with compounds for 30 min. Cells were then stressed by adding NaAsO₂ or thapsigargin diluted in 100 μ L media to a final concentration of 500 μ M or 5 μ M, respectively and incubated for 60 min. Cells were then fixed, stained with DAPI and imaged at 40 \times magnification on an Opera Phenix high content imaging system (Perkin Elmer).

iPS-MN puromycin stress and recovery assays

TARDBP mutant, FUS mutant and control iPS-MNs were generated from human induced pluripotent stem cells as described above and seeded into pre-coated 384-well plates as described above for hit compound inhibition of SGs in iPS-MNs. Cells were stressed by adding puromycin diluted in 20 μ L of iPS-MN media to a final concentration of 5 μ g/mL. After incubation with puromycin for 24 hours, three half-media changes with iPS-MN media were performed to wash out the stressor. The iPS-MNs were then incubated for 24 hours at 37°C, 5% CO₂, after which cells were fixed and DAPI stained. iPS-MNs were also fixed at intermediate time points to generate a time course for SG and TDP-43 puncta assembly/disassembly dynamics during puromycin stress and stress recovery. G3BP1 and TDP-43 were stained by IF according to the procedure described above for IF staining of SG-enriched fractions. iPS-MNs were imaged as described above for robotic imaging of primary screen plates. SG-enriched fractions were also isolated from iPS-MNs following the protocol described above.

iPS-MN stress and recovery with compounds

TARDBP mutant, *FUS* mutant and control iPS-MNs were generated from human induced pluripotent stem cells as described above and seeded into precoated 384-well plates as described above for hit compound inhibition of SGs in iPS-MNs. Cells were pre-treated with mitoxantrone, digitoxin or pyrvinium diluted in 20 μ L of iPS-MN media to a final concentration of 2 μ M and incubated at 37°C, 5% CO₂ for 60 min, after which cells were stressed by adding puromycin diluted in 40 μ L of iPS-MN media to a final concentration of 5 μ g/mL. After incubation with puromycin for 6 hours, three half-media changes with iPS-MN media were performed to wash out the stressor and mitoxantrone. The cells were then incubated for 7 hours at 37°C, 5% CO₂ to recover from stress. Cells were fixed at the unstressed (0h), stressed (7h) and recovery (14h) time points and DAPI stained. G3BP1 and TDP-43 were stained by IF according to the procedure described above for IF staining of SG-enriched fractions. iPS-MNs were imaged as described above for robotic imaging of primary screen plates.

Neuronal survival assay with compounds

Primary cortical neurons were harvested from E17 mouse embryos, cultured in Neurobasal medium with B27 and GlutaMAX, and grown for 2 days *in vitro* in 384-well plates. Neurons were co-transfected with pGW1-mApple and pGW1-EGFP or pGW1-TDP-43(M337V)-EGFP using Lipofectamine 2000 (Thermo Fisher). Two hours after transfection, neurons were treated with digitoxin, doxorubicin, ISRIB, mitoxantrone or quinacrine at various concentrations from 1 nM to 8 μ M in 0.2% DMSO. Controls were treated with 0.2% DMSO only. 16 wells per condition were used. Starting the next day, primary neurons were imaged daily for three days by using a custom-built robotic microscope with a Nikon Eclipse Ti base and Andor Zyla 4.2 camera ([Arrasate et al., 2004](#); [Barmada et al., 2010](#)). Images were montaged and individual mApple+ neurons were segmented using custom software. Neuronal survival was determined by a neural network trained to classify individual neurons as alive or dead (manuscript in preparation). Raw survival data was used to calculate a cumulative death rate, given by the cumulative ratio of dead neurons to alive neurons, and then averaged across wells of the same treatment. Cumulative death rate curves were fit to a linear mixed effects model with each well as a random effect and an interaction between treatment and time as a fixed effect. P values were adjusted for multiple comparisons by the Holm-Bonferroni method.

QUANTIFICATION AND STATISTICAL ANALYSIS

For each experiment, the arithmetic mean of replicates is represented in quantification figures. The statistical tests, significance levels, exact number and type (biological versus experimental) of replicates performed and dispersion measures represented (SD versus sem) are denoted in the figure legends.

Statistical analysis of screen data

SG-modulating compounds were defined as hits that significantly decrease or increase one or more of three metrics:

1. Amount of SG formation per cell, defined as the total image area enclosed in SGs divided by the total image area enclosed in nuclei (SG area/nuclei area).
2. Number of SGs per cell, defined as the number of SG puncta divided by the total image area enclosed in nuclei (SG count/nuclei area).
3. Average size of SGs, defined as the total image area enclosed in SGs divided by the number of SG puncta (SG area/SG count).

To identify hit compounds for these three metrics, a custom computational pipeline, Statistical Workflow for Identification of Molecular Modulators of ribonucleoproteins by Random variance modeling (SWIMMER; open source and available publicly on yeolab github page: <https://github.com/YeoLab>), was built following standard statistical practices for high-throughput screening ([Birmingham et al., 2009](#); [Malo et al., 2006](#)). Data from each compound library screened in each cell type was run separately through the pipeline. The pipeline begins by interpolating sporadic missing values via K-nearest neighbors missing data imputation, using K = 10 nearest neighbors and Euclidean distances ([Aittokallio, 2010](#)). To reduce batch effects, the pipeline then performs a two-way median polish, alternating across rows and columns over 10 iterations ([Malo et al., 2006](#); [Mosteller and Tukey, 1977](#)). Next, normalization is performed by computing b-scores, in which post-polish residuals are divided by the median absolute deviation of all post-polish residuals of the screen ([Brudeau et al., 2003](#)). To increase the power of hypothesis tests performed on the b-scores and therefore improve calling of screen hits, the screen was performed across two to four biological duplicates, sample variances across the replicate b-scores were computed and an inverse gamma distribution was fitted to the distribution of sample variances ([Wright and Simon, 2003](#)). Fitting an inverse gamma distribution enables performing a modified one sample Student's t test which has increased statistical power for each screen compound ([Birmingham et al., 2009](#); [Malo et al., 2006](#)). This modified t test involves computing for each compound a modified t-statistic $t = (\bar{x} - \mu_0 / \tilde{s} \sqrt{1/K})$, where \bar{x} is the sample mean for the compound across K biological replicate b-scores, μ_0 is the mean under the null hypothesis and \tilde{s}^2 is the modified sample variance for the compound across K biological replicate b-scores. In the present SG screen, $\mu_0 = 0$, $K = 2$ and $\tilde{s}^2 = ((K - 1)s^2 + 2a(ab)^{-1})/(K - 1) + 2a$, where s^2 is the unmodified sample variance across K biological replicate b-scores and a and b are the fitted parameters of the inverse gamma distribution. Using these modified one sample Student's t tests, hits were called using a significance cutoff of $\alpha = 0.001$. Given that this was the

first pass analysis of the screen, we prioritized avoiding false negatives over accumulating false positives, since we aimed to eliminate the latter through subsequent counterscreens and secondary validations. Calling hits using the Bonferroni procedure to control for the family-wise error rate or the Benjamini-Hochberg procedure to control for the false discovery rate proved too stringent and resulted in too many false negatives, as determined by manual examination of the screen raw images. Instead, we performed quality control (QC) for called hits by manual examination of the screen raw images for imaging artifacts or confounding effects such as auto-fluorescence or out-of-focus wells. Screen hits that passed QC were manually annotated with the compound names, skeletal formulae and previously reported cellular targets of the compounds using the National Center for Biotechnology Information PubChem database.

Computing Z' for the primary screen assay

To estimate whether the screen assay has adequate sensitivity and specificity for detecting hits in a high-throughput screening paradigm, the Z' was computed for the screen assay in each cell type: $Z' = 1 - (3(\hat{\sigma}_p + \hat{\sigma}_n)/|\hat{\mu}_p - \hat{\mu}_n|)$, where $\hat{\sigma}_p$ and $\hat{\sigma}_n$ are the SD for the positive and negative controls, respectively and $\hat{\mu}_p$ and $\hat{\mu}_n$ are the sample means for the positive and negative controls, respectively. The Z' is therefore a measure of the signal-to-noise in the screen assay and an assay is suitable for high-throughput screen if the Z' is greater than 0.5 (Zhang et al., 1999).

Estimating IC₅₀s of SG inhibiting compounds

IC₅₀s were estimated from logistic functions fitted to the dose response data of SG inhibiting compounds. Least-squares regression was used to fit logistic functions of the type: $f(x) = (L/1 + e^{-k(x - x_0)})$, where L is the maximum value of the curve, k is the steepness of the curve and x_0 is the midpoint of the curve. From these fitted logistic functions, the IC₅₀ estimates are therefore the fitted x_0 parameters, representing the midpoints of the dose-response transfer curves.

Manders' co-localization measure

Images were first pre-processed in ImageJ, to subtract background using the rolling ball method with a radius of 50 pixels (required for subsequent Manders' Correlation Coefficient calculations) and then to transform the dynamic range of the brightness to 2-10 (arbitrary units). Co-localization of G3BP1-GFP SGs with RBPs probed with Alexa-555 conjugated antibodies was then quantified using Manders' algorithm in the Fiji plugin Coloc2 to calculate the unthresholded Manders' Correlation Coefficient between the GFP fluorescence channel image and the Alexa-555 fluorescence channel image (Manders et al., 1993; Schindelin et al., 2012). In this way, co-localization is defined as the fraction of G3BP1-GFP-positive pixels that coincide with Alexa-555-positive pixels.

DATA AND CODE AVAILABILITY

Screen hit identification pipeline

To identify hit compounds which modulate SGs, a custom computational pipeline, Statistical Workflow for Identification of Molecular Modulators of ribonucleoproteins by Random variance modeling (SWIMMER), was built following standard statistical practices for high-throughput screening (Birmingham et al., 2009; Malo et al., 2006). It is open source available publicly on yeolab github page: <https://github.com/YeoLab>.

Screen raw data

The accession number for the screen raw data reported in this paper is Mendeley Data: <https://doi.org/10.17632/6jpt8b7g8t.1>

Raw and analyzed data

The accession number for the raw and analyzed data reported in this paper is Mendeley Data: <https://doi.org/10.17632/6jpt8b7g8t.1>